

# Clustering of Galaxies in a Hierarchical Universe: I. Methods and Results at $z = 0$

Guinevere Kauffmann, Jörg M. Colberg, Antonaldo Diaferio & Simon D.M.  
White

*Max-Planck Institut für Astrophysik, D-85740 Garching, Germany*

## Abstract

We introduce a new technique for following the formation and evolution of galaxies in cosmological N-body simulations. Dissipationless simulations are used to track the formation and merging of dark matter halos as a function of redshift. Simple prescriptions, taken directly from semi-analytic models of galaxy formation, are adopted for gas cooling, star formation, supernova feedback and the merging of galaxies within the halos. This scheme enables us to explore the clustering properties of galaxies and to investigate how selection by luminosity, colour or type influences the results. In this paper, we study the properties of the galaxy distribution at  $z = 0$ . These include B and K-band luminosity functions, two-point correlation functions, pairwise peculiar velocities, cluster mass-to-light ratios,  $B - V$  colours and star formation rates. We focus on two variants of a cold dark matter (CDM) cosmology: a high-density ( $\Omega = 1$ ) model with shape-parameter  $\Gamma = 0.21$  ( $\tau$ CDM), and a low-density model with  $\Omega = 0.3$  and  $\Lambda = 0.7$  ( $\Lambda$ CDM). Both models are normalized to reproduce the I-band Tully-Fisher relation of Giovanelli et al. (1997) near a circular velocity of  $220 \text{ km s}^{-1}$ . Our results depend *strongly* both on this normalization and on the adopted prescriptions for star formation and feedback. Very different assumptions are required to obtain an acceptable model in the two cases. For  $\tau$ CDM, efficient feedback is required to suppress the growth of galaxies, particularly in low-mass field haloes. Without it, there are too many galaxies and the correlation function exhibits a strong turnover on scales below 1 Mpc. For  $\Lambda$ CDM, feedback must be weaker, otherwise, too few  $L_*$  galaxies are produced and the correlation function is too steep. Although neither model is perfect both come close to reproducing most of the data. Given the uncertainties in modelling some of the critical physical processes, we conclude that it is not yet possible to draw firm conclusions about the values of cosmological parameters from studies of this kind. Further observational work on global star formation and feedback effects is required to narrow the range of possibilities.

Keywords: galaxies: formation; galaxies:halos; cosmology:large-scale structure; cosmology: dark matter

# 1 Introduction

A major motivation for carrying out N-body simulations of large-scale structure formation is to test theories for the origin of structure and to estimate cosmological parameters, such as the density  $\Omega$ , or the cosmological constant  $\Lambda$ . Physically accurate identification of the positions, velocities and intrinsic properties of galaxies is necessary if such simulations are to provide estimates of statistics such as the spatial and velocity correlations of galaxies, which can be reliably compared with observations.

Dissipationless simulations of gravitational clustering using tens of millions of particles are now carried out routinely on parallel supercomputers. Such simulations are able to resolve the formation and evolution of the dark matter halos of typical galaxies over cosmologically significant volumes. However, once these galaxy-sized halos merge to form larger structures, such as groups or clusters, they are quickly disrupted and are no longer distinguishable as separate entities within the more massive systems. This is commonly referred to as the “overmerging problem”. Several recent papers have demonstrated that with sufficient force and mass resolution ( $\sim 1-3$  kpc and  $10^8-10^9 M_\odot$ ) the central cores of many simulated galaxy halos do “survive” in groups and clusters, but even with this resolution, substructure is still erased in the dense central regions (Tormen, Diaferio & Syer 1998; Ghigna et al 1998; Klypin et al. 1998).

Dissipationless simulations do not address the fact that on scales of a few kiloparsecs, gas-dynamical processes are known to play a key role in determining the structure of galaxies. Numerical simulations that treat the physics of the baryonic component can be used to overcome this deficiency. Indeed, it has been demonstrated that when radiative cooling is included, many individual dense knots of cold gas do survive within a present-day cluster (e.g. Carlberg, Couchman & Thomas 1990; Katz, Hernquist & Weinberg 1992; Navarro & White 1994; Evrard, Summers & Davis 1994; Frenk et al. 1996). Such simulations require a heavy investment of CPU time and with present-day computer technology, it is difficult to follow the formation of galaxies in volumes that are large enough to study large-scale structure. In addition, the galaxies themselves are very poorly resolved and processes such as star formation and supernova feedback still have to be put into the simulations “by hand” because they are strongly influenced by structure much smaller than the resolution limit.

In this paper, we introduce a technique for following the formation and evolution of galaxies in cosmological N-body simulations. Dissipationless simulations are used to track the formation and merging of dark matter halos as a function of redshift. The most bound particle in each halo is identified as the site where cold gas condenses and forms stars. Later, when two or more halos merge in the simulation, these particles maintain their identities as separate galaxies except they can merge with the new central object on a timescale set by dynamical friction. Simple prescriptions are adopted for gas cooling rates, star formation and supernova feedback. These are based on simplified models of the physical processes or on simulation results and are taken directly from earlier *semi-analytic* studies of galaxy formation. These used analytic models rather than N-body simulations to specify the merging histories of dark matter halos for a given set of cosmological initial conditions. Such semi-analytic models were able to account for many aspects of the present-day galaxy population, for example the luminosities, colours and morphologies of galaxies and the observed correlation of these properties with environment (White & Frenk 1991; Lacey & Silk 1991; Kauffmann, White & Guiderdoni

1993; Cole et al 1994; Baugh, Cole & Frenk 1996b; Somerville & Primack 1998). In addition, semi-analytic models have been used to study the evolution of the galaxy population to high redshift and to make predictions for faint galaxy counts, for the redshift distributions of faint galaxies, for the evolution of the morphology-density relation and for the abundance and properties of galaxies and damped Ly $\alpha$  absorbers at high redshifts ( Lacey et al. 1993; Kauffmann, Guiderdoni & White 1994; Heyl et al 1995; Kauffmann 1995a,b; Baugh, Cole & Frenk 1996a; Kauffmann 1996a,b; Kauffmann & Charlot 1998; Baugh et al 1998; Mo, Mao & White 1998).

The combination of semi-analytic galaxy formation models with cosmological N-body simulations results in an important advance. It becomes possible to track the positions and velocities of galaxies as a function of time, in addition to properties such as stellar mass, luminosity, colour and morphology. One can then compute the standard statistical measures used to quantify the clustering of galaxies, such as the two-point correlation function or the pairwise peculiar velocities, and investigate how the selection of galaxies by luminosity, colour or type influences the results. One can extract mock catalogues from the simulations in order to study the clustering properties of galaxies in redshift space. One can investigate whether the galaxy distribution is *biased* relative to that of the dark matter and how this bias affects attempts to measure the density parameter  $\Omega$  from galaxy surveys. Finally, one can also study how the clustering of galaxies evolves with redshift.

Some, but not all of these issues have been explored in previous papers. White et al (1987) assumed that a galaxy formed at the centre of a halo during its initial collapse and then tracked the positions of the central particles as a function of time. The circular velocities of galaxies were given by the the circular velocities of the halos in which they formed. Galaxies were also able to merge if they approached within a certain critical radius of each other. White et al (1987) demonstrated that at the present day, galaxies with high circular velocities cluster more strongly than galaxies with low circular velocities. Van Kampen & Katgert (1997) used a similar approach to follow the formation of galaxies within N-body simulations of cluster formation. In their scheme, each group of bound particles in virial equilibrium was replaced by a single massive particle with a softening corresponding to the radius of the group. The studies of White et al and Van Kampen & Katgert did not include any scheme for star formation and no attempt was made to compute the luminosities or colours of the galaxies in the simulation.

Modelling of cooling, star formation, feedback and stellar evolution is included in the cosmological Eulerian grid calculations of Cen & Ostriker (1992,1993). Even though these calculations have insufficient resolution to follow the collapse and dynamics of galaxy halos, and so cannot reliably identify individual galaxies, Cen & Ostriker were able to address some of the issues we discuss in the present paper (e.g. bias and the dependence of clustering on galaxy age). A number of their conclusions prefigure our own.

The results of semi-analytic models have been used to place galaxies within individual outputs of N-body simulations with higher resolution. Analytic methods are used to compute the luminosity function of galaxies within dark matter halos of given mass  $M$  and galaxies are then assigned randomly to particles in each simulated halo of this mass. Kauffmann, Nusser & Steinmetz (1997) used this method to study present-day bias as a function of galaxy luminosity, colour and type, while Governato et al. (1998) used the same technique to analyze the clustering properties of Lyman break galaxies at redshifts  $\sim 3$ . The disadvantage is that the properties of the galaxies within each simulated halo do not depend on the merging history of

that particular halo. Correct results are only obtained if an average is taken over many halos. Furthermore there is no detailed correspondence between the galaxy populations assigned to the simulations at different times so that many questions about the evolution of galaxy clustering cannot be directly addressed. Finally, the method is subject to all the inaccuracies of the Press-Schechter theory and its extensions (see section 5 below). It is therefore advantageous to compute the merging histories of dark halos directly from the simulations. This has been done by Roukema et al. (1997) who studied the evolution of both halos and galaxies in simulations with scale-free initial conditions. Their method included prescriptions for star formation and they were able to demonstrate that different assumptions could strongly affect the predicted number density of low-luminosity galaxies.

This paper is the first in a series studying the properties of galaxies identified in N-body simulations with cold dark matter (CDM) initial conditions. These simulations are much larger than those analyzed in previous work and are able to resolve the detailed merging history of the dark matter halo of an  $L_*$  galaxy within a volume of  $\sim 10^7$  Mpc<sup>3</sup>. We first describe the simulations and the methods used to construct halo merging trees. We outline the prescriptions adopted to model cooling, star formation, supernova feedback, galaxy-galaxy merging and the evolution of the stellar populations within galaxies. We show how the luminosity functions of galaxies in the simulations compare with those derived from the analytic merging trees of Kauffmann & White (1993).

We then study the properties of the galaxy distribution at  $z = 0$ . These include the I-band Tully-Fisher relation, B and K-band luminosity functions, the two-point spatial correlation function  $\xi(r)$ , two-point velocity correlations, cluster  $M/L$  ratios, the  $B - V$  colour distributions of galaxies of different types, and the predicted  $H\alpha$  luminosity function. We focus on two variants of a cold dark matter (CDM) cosmology: a high-density ( $\Omega = 1$ ) model with shape-parameter  $\Gamma = 0.21$  ( $\tau$ CDM), and a low-density model with  $\Omega = 0.3$  and  $\Lambda = 0.7$  ( $\Lambda$ CDM). The normalization  $\sigma_8$  is chosen to match the observed abundance of rich clusters in the Universe at  $z = 0$ . The parameters controlling star formation and supernova feedback are set so that galaxies with circular velocities of 220 km s<sup>-1</sup> have an I-band magnitude consistent with the Tully-Fisher relation of Giovanelli et al (1997).

We show that different ways of treating star formation and feedback in the models have a strong influence both on the galaxy luminosity function and on the slope and amplitude of the two-point correlation function. In order for the high-density  $\tau$ CDM model to come close to matching the observations, we have to suppress the formation of galaxies in low-mass halos in the field. This is achieved by assuming that supernova feedback is so efficient that it can eject a substantial fraction of the baryons from the potential wells of low-mass dark matter halos. Even so, the model still produces an excess of very bright galaxies in groups and clusters. The low-density  $\Lambda$ CDM model produces *too few* star-forming field galaxies, even if feedback is weak and gas never escapes from dark halos. We have also investigated the effect of dust extinction on predictions for the colour distributions and clustering properties of galaxies. Given the uncertainties in modelling some of the critical physical processes, we conclude that we cannot reliably constrain the values of cosmological parameters using the properties of the galaxy distribution at  $z = 0$ .

## 2 The simulations

The simulations we use were run as a part of the GIF project, a joint effort of astrophysicists from Germany and Israel. Its primary goal is to study the formation and evolution of galaxies in a cosmological context using semi-analytical galaxy formation models embedded in large high-resolution  $N$ -body simulations. The code used for the GIF simulations is called Hydra. It is a parallel adaptive particle-particle particle-mesh (AP<sup>3</sup>M) code (for details on the code, see Couchman, Thomas, & Pearce 1995; Pearce & Couchman 1997). The current version was developed as part of the VIRGO supercomputing project and was kindly made available by them for the GIF project. The simulations were started on the CRAY T3D at the Computer Centre of the Max-Planck Society in Garching (RZG) on 128 processors. Once the clustering strength required a finer base mesh and so an even larger amount of total memory, they were transferred to the T3D at the Edinburgh Parallel Computer Centre (EPCC) and finished on 256 processors.

A set of four simulations with  $N = 256^3$  and with different cosmological parameters was run (Table 1). All the simulations are “cluster normalized”. White, Efstathiou, & Frenk (1993) introduced this way of fixing the amplitude by determining  $\sigma_8$ , the square root of the variance of the density field smoothed over  $8 h^{-1}$  Mpc spheres, such that the observed abundance of high-mass clusters is matched. More recent determinations of  $\sigma_8$  using the observed cluster X-ray temperature function (Eke, Cole, & Frenk 1996; Viana & Liddle 1996) yield similar results. For the low-density GIF simulations, the result by Eke et al. (1996) was taken. For the  $\Omega = 1$  simulations, slightly larger values than suggested by Eke et al. (1996) were adopted, according to the earlier result by White et al. (1993).

The parameters shown in Table 1 were chosen not only to fulfil cosmological constraints, but also to allow a detailed study of the clustering properties at very early redshifts. The masses of individual particles are  $1.0 \times 10^{10} h^{-1} M_\odot$  and  $1.4 \times 10^{10} h^{-1} M_\odot$  for the high- and low- $\Omega$  models, respectively. The gravitational softening was taken to be  $30 h^{-1}$  kpc. Gravitational lensing by clusters in this set of four models has been studied by Bartelmann et al (1998).

In this paper we focus on two of the models:  $\tau$ CDM and  $\Lambda$ CDM. Both have shape parameter  $\Gamma = 0.21$ . A value of  $\Gamma = 0.21$  is usually preferred by analyses of galaxy clustering, for example Peacock & Dodds (1994). This is achieved in the  $\tau$ CDM model, despite  $\Omega = 1$  and  $h = 0.5$ , by assuming that a massive neutrino (usually taken to be the  $\tau$  neutrino) was present during the very early evolution of the Universe and came to dominate the energy density for a short period. It then decayed into lighter neutrinos which are still relativistic, thus delaying the epoch when matter again started to dominate over radiation. The neutrino mass and lifetime are chosen such that  $\Gamma = 0.21$ . For a detailed description of such a model see White, Gelmini, & Silk (1995).

## 3 Construction of Halo Merger Trees and Identification of Galaxy Positions

In order to follow the merging history of dark matter halos in the simulations, we store particle positions and velocities at 50 different output times, spaced in equal logarithmic intervals in redshift from  $z = 20$  to  $z = 0$ . The construction of merger trees from these simulation outputs

involves the following steps.

A friends-of-friends group-finding program is used to locate virialized halos. We adopt a linking length which is 0.2 times the mean interparticle separation. Only halos containing at least 10 particles are included in our halo “catalogues”. Tests show that 10-particle halos are stable systems. More than 95 % of 10 particle halos identified at one output time are still located within groups of 10 particles or more at subsequent times. By “located”, we mean that more than 80% of the particles in one halo are present in the *same halo* at the later time. Halos with masses below about 7 particles do not survive over many output times according to this criterion.

The lowest luminosity galaxy that we are able to resolve in these simulations thus corresponds to a galaxy in a halo with 10 particles or  $\sim 10^{11}h^{-1}M_{\odot}$ . In these models, the Milky Way halo has a mass of  $\sim 2 \times 10^{12}h^{-1}M_{\odot}$ , so the faintest resolved galaxies are roughly a tenth as bright (i.e. comparable in luminosity to the Large Magellanic Cloud).

We then compute a set of physical quantities for all the halos in the catalogues. These are:

1. *the central particle index*. This is the index of the most-bound particle in the halo. This particle has particular significance as it marks the position of the *central galaxy* of the halo, ie the galaxy onto which gas cools and where it forms stars.
2.  $R_{vir}$ , the virial radius, defined as the distance from the central particle within which the overdensity of dark matter is 200 times the background density.
3.  $M_{vir}$ , the virial mass. This is the mass of dark matter contained within  $R_{vir}$ .
4.  $V_c$ , the circular velocity ( $V_c = (GM_{vir}/R_{vir})^{1/2}$ ).

We begin with the first simulation output that has at least one halo with 10 particles or more. The central particles of these halos mark the locations of the first galaxies identified in the simulation. We then go to the next output time and loop through all the halos in the catalogue, searching for *progenitor halos* at the previous time. A halo at redshift  $z_1$  is defined to be a progenitor of a halo at redshift  $z_0 < z_1$ , if

1. more than half its particles are included in the halo at redshift  $z_0$ ; and
2. its central particle is also included in that halo.

The most massive progenitor of a halo has a special status – the properties of its central galaxy are transferred to the central galaxy of the new halo. We thus *reposition* the central galaxy at each output time. The particle index corresponding to the central galaxy changes, but its associated mass and luminosity evolve in a smooth fashion. This procedure ensures that cold gas always settles at the centre of a halo. The central galaxies of less massive progenitors become *satellites*. The particle index of a satellite galaxy then remains fixed until the present day. A satellite is said to “belong” to a halo if its particle index is among those linked together by the groupfinder.

This procedure is repeated at every output time until  $z = 0$ . At each timestep, and for all the halos in the associated catalogue, we store the following information:

1. The index of the central particle of the largest progenitor of the halo (zero if the halo had no progenitors).
2. The indices of all satellite galaxies contained within the halo (particles that were central galaxies of smaller halos at earlier times, and that are now incorporated within the present halo)

This is sufficient to follow the evolution and merging of all galaxies within the simulation volume using the scheme outlined in the next section.

Occasionally a galaxy identified at one time is not included within any halo at a subsequent time. This may happen for the following reasons:

1. A halo that was above the 10-particle resolution limit at one time, may fall below this limit at a later time. In this case, there is a central galaxy that does not belong to any halo in the next simulation output.
2. Satellite galaxies are occasionally “ejected” out of halos, particular during mergers. In most cases, the satellite will fall back into the halo at a later time.

We keep an index list of these “lost” galaxies, checking at each subsequent output time to see whether they have been re-incorporated into a halo. If the recovered particle was previously a central galaxy, its properties are transferred to the central galaxy of the new halo if the difference in mass between the old and new halos is small (less than a factor 2). Otherwise, the recovered particle becomes a satellite galaxy within the new halo. Recovered satellite galaxies simply join the satellite population of the new halo. Note that lost galaxies comprise only a few percent of the total galaxy population at all times. Moreover, most of them are faint.

## 4 The Physical Processes Governing Galaxy Formation

Our treatment of the physical processes governing galaxy formation is very similar to that described in Kauffmann, White & Guiderdoni (1993, KWG) and in White & Frenk (1991). The reader is referred to these papers for more detailed discussion and for derivations of some of the equations. Some of our prescriptions, in particular those for feedback and for galaxy-galaxy merging, have changed since these papers were published. We have also incorporated a number of extra features, such as dust extinction and starbursts during galaxy-galaxy mergers. For completeness, we now present a summary of our prescriptions for the various physical processes. A detailed discussion of how these are implemented is given in section 4.8.

### 4.1 Gas Cooling

We adopt the simple model for cooling first introduced by White & Frenk (1991). For simplicity, dark halos are modelled as isothermal spheres truncated at their virial radius  $R_{vir}$ . We assume that the hot gas *always* has a distribution that exactly parallels that of the dark matter. The total mass of hot gas in the halos is given by

$$M_{hot} = \Omega_b M_{vir} - M_* - M_{cool} - M_{eject}, \quad (1)$$

where  $\Omega_b$  is the baryon density of the Universe,  $M_{vir}$  is the virial mass of the halo,  $M_*$  is the total mass of stars that have formed in the halo,  $M_{cool}$  is the total cold gas contained in the halo and  $M_{eject}$  is the mass of gas ejected out of the halo by supernova feedback (see section 4.3).

The gas temperature can then be derived from the circular velocity of the halo using the equation of hydrostatic equilibrium:

$$T = 35.9(V_c/\text{kms}^{-1})^2\text{K} \quad (2)$$

At each radius in the halo, we define a local cooling time through the ratio of the specific energy content to the cooling rate  $\Lambda(t)$ .

$$t_{cool}(r) = \frac{3\rho_g(r)}{2\mu m_p} \frac{kT}{n_e^2(r)\Lambda(t)} \quad (3)$$

where  $\rho_g(r)$  is the gas density,  $n_e(r)$  is the electron density,  $m_p$  is the proton mass and  $\mu m_p$  is the molecular weight of the gas. In this paper, we do not include chemical enrichment. The gas is assumed to have solar metallicity at all times and we use the solar metallicity cooling curve in figure 9.9 of Binney & Tremaine (1987). (see Kauffmann 1996b and Kauffmann & Charlot 1998 for a description of models including chemical evolution).

At a given redshift  $z$ , a cooling radius  $r_{cool}$  can be defined as the radius within the halo where the cooling time is equal to the age of the Universe. For the case of an Einstein-de Sitter cosmology,

$$t_{cool}(r_{cool}) = \frac{2}{3}H_0^{-1}(1+z)^{-3/2}. \quad (4)$$

At high redshifts, for small halos, and for high gas fractions, the cooling radius is larger than the virial radius of the halo. We assume that in the absence of supernovae, all the hot gas in the halo would settle to the centre on a timescale given by the halo dynamical time ( $R_{vir}/V_c$ ). We thus write the instantaneous cooling rate as

$$\dot{M}_{cool}(V_c, z) = \frac{M_{hot}V_c}{R_{vir}}. \quad (5)$$

The gas content of the halo is further affected by feedback (see next section) and by the infall of new material, which we determine directly from the merging trees.

At later times, for larger halos, and for low gas fractions, the cooling radius lies inside the virial radius and the rate at which gas cools is calculated using the equation

$$\dot{M}_{cool}(V_c, z) = 4\pi\rho_g(r_{cool})r_{cool}^2 \frac{dr_{cool}}{dt}. \quad (6)$$

As has been shown in KWG and in Aragon-Salamanca, Baugh & Kauffmann(1998), for massive halos the cooling rates given by equation 6 lead to the formation of central cluster galaxies that are too bright and too blue to be consistent with observation if the cooling gas is assumed to form stars with a standard initial mass function. It should be noted that cooling flows of hundreds of solar masses per year are *observed* in a number of clusters (see for example Fabian, Nulsen & Canizares 1991; Allen & Fabian 1997), but that the fate of the cooling gas remains a mystery. One hypothesis is that it may condense into cold clouds instead of stars

(Ferland, Fabian & Johnstone 1994). In our models, we assume the gas cooling in halos with  $V_c > 350 \text{ km s}^{-1}$  does not form visible stars. Note that this is the lowest circular velocity at which we can suppress star formation in cooling flows without destroying our fit to the Tully-Fisher relation (see section 6.2).

## 4.2 Star Formation

As in KWG, we adopt a simple star formation law of the form

$$\dot{M}_* = \alpha M_{\text{cold}}/t_{\text{dyn}}, \quad (7)$$

where  $\alpha$  is a free parameter and  $t_{\text{dyn}}$  is the dynamical time of the galaxy. For a central galaxy in a halo, the dynamical time is given by

$$t_{\text{dyn}} = 0.1 R_{\text{vir}}/V_c. \quad (8)$$

For disk galaxies, this is motivated by noting that, if gas collapses to a centrifugally supported state within an isothermal halo while conserving angular momentum, the contraction factor is  $\sim 2\lambda$ , where  $\lambda$  is the spin parameter of the gas, assumed to be the same as for the halo. N-body simulations find that  $\lambda$  scatters around a value of  $\sim 0.05$ . For a satellite galaxy,  $t_{\text{dyn}}$  is held fixed at the value when the galaxy was last a central galaxy.

It should be noted that according to the simple spherical collapse model, the virial radius of a dark matter halo scales with circular velocity and with redshift as  $R_{\text{vir}} \propto V_c(1+z)^{-3/2}$ , reflecting the fact that halos are smaller and denser at earlier epochs. This means that  $t_{\text{dyn}}$  is independent of the circular velocity of the halo, but will decrease at higher redshift, so star formation rates are higher in halos of the same cold gas content at high  $z$ .

The star formation law in equation 7 has received considerable *empirical* support from a recent study of the star formation rates and gas masses in 61 nearby spiral galaxies and 36 “starburst” systems by Kennicutt (1997), who finds that such a law can fit the data over several orders of magnitude in star formation rate and gas density. In normal spirals, about 10 percent of the available gas is turned into stars per orbital time.

## 4.3 Feedback from Supernovae

The effect of energy ejected by supernova explosions into the interstellar medium of a galaxy has profound implications for the observed properties of galaxies. As shown by Cole et al (1994) and Somerville & Primack (1998), strong feedback in low-mass galaxies is required to fit the flat ( $\alpha > -1.3$ ) faint-end slope of the galaxy luminosity function. Kauffmann & Charlot (1998) have demonstrated that substantial feedback in *massive* ( $\sim L_*$ ) galaxies is also needed to fit the observed slope of the colour-magnitude relation of elliptical galaxies. Unfortunately, both theoretical and observational understanding of how feedback operates in different types of galaxies is extremely limited at present, so we have no option other than to experiment with a variety of different prescriptions in order to see what difference they make to our results.

Using basic energy-conservation arguments, it is possible to estimate how much cold gas could be reheated to the virial temperature of the halo for a given mass of stars formed in

the galaxy. For the Scalo (1986) initial mass function we use to model the evolution of the stellar populations in our galaxies (see section 4.6), the number of supernovae expected per solar mass of stars formed is  $\eta_{SN} = 5 \times 10^{-3} M_{\odot}^{-1}$ . The kinetic energy of the ejecta from each supernova,  $E_{SN}$ , is about  $10^{51}$  erg. If a fraction  $\epsilon$  of this energy is used to reheat cold gas to the virial temperature of the halo, the amount of cold gas lost in time  $\Delta t$  can be estimated as

$$\Delta M_{reheat} = \epsilon \frac{4 \dot{M}_* \eta_{SN} E_{SN}}{3 V_c^2} \Delta t. \quad (9)$$

In the models,  $\epsilon$  is treated as a free parameter.

One major uncertainty is whether the gas heated by supernova explosions will leave the halo. In our previous work, reheated gas was always retained within the halo. Another possibility is that reheated gas will be ejected out of halo. In the models of Cole et al (1994), reheated gas was removed until the halo grew in mass by a factor of two or more, whereupon it was added once again to the hot gas component. The re-incorporation of expelled gas at a later time ensured that the total baryonic mass in halos was conserved and that the baryon fraction in clusters was close to the global value.

In this paper, we will experiment with both feedback prescriptions. We call the model in which reheated gas is always trapped within the halo the “retention” model. The model in which reheated gas is expelled from the halo will be called the “ejection” model. According to our star formation prescription, stars form efficiently in low mass halos at high redshifts. In the ejection model, the energy injected into the ISM by the first generation of star formation is sufficient to expel most of the gas from the halo. The star formation rate then drops and the galaxy fades until the gas is re-incorporated on the next collapse. Stars in low-mass galaxies are thus formed in a series of “bursts” associated with each factor 2 doubling in halo mass. This bursting behaviour is much less pronounced for massive galaxies, since their potential wells are deeper and much less gas will be expelled (equation 9).

The effect of the two feedback prescriptions on the typical star formation history of a  $L_*$  galaxy (more specifically, the central galaxy of a halo with  $V_c = 220 \text{ km s}^{-1}$ ) is shown in figure 1. As can be seen, the ejection prescription results in both higher and more irregular rates of star formation at high redshift when the galaxies reside within low- $V_c$  halos. At low redshifts, the halo potential wells are deeper and so more effective at retaining the gas heated during supernova explosions. The star formation rates for the two prescriptions thus do not differ very much at the present epoch.

## 4.4 Merging of Galaxies

N-body plus smoothed particle hydrodynamic (SPH) simulations of the assembly of galaxies in a hierarchical Universe show that as dark matter halos coalesce, the embedded disk galaxies merge on a timescale that is consistent with dynamical friction estimates based on their total (gas + surrounding dark matter) mass (Navarro, Frenk & White 1995). The dynamical friction timescale, in the form given by Binney & Tremaine (1987) is:

$$T_{dynf} = \frac{1}{2} \frac{f(\epsilon)}{GC \ln(\Lambda)} \frac{V_c r_c^2}{M_{sat}}, \quad (10)$$

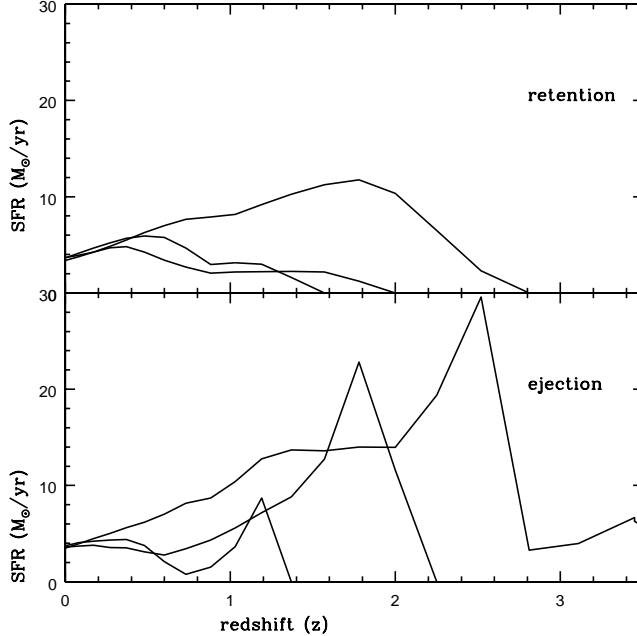


Figure 1: A comparison of the star formation histories for 3 central galaxies in halos of  $V_c = 220 \text{ km s}^{-1}$  for the retention and the ejection feedback schemes.

where  $V_c$  is the circular velocity of a singular isothermal sphere representing the primary halo,  $M_{sat}$  is the mass of the orbiting satellite,  $\ln(\Lambda)$  is the Coulomb logarithm which we approximate as  $\ln(M_{vir}/M_{sat})$ . The function  $f(\epsilon)$  allows for the angular momentum of the satellite's orbit, expressed in terms of the circularity parameter  $\epsilon = J/J_c(E)$ , the ratio of the angular momentum of the satellite to that of a circular orbit with the same energy. Lacey & Cole (1993) show that  $f(\epsilon) \simeq \epsilon^{0.78}$  for  $\epsilon > 0.02$ . Finally,  $r_c(E)$  is the radius of the circular orbit with the same energy as the satellite orbit. Navarro, Frenk & White show that equation 10 provides, on average, a fair estimate of the merger timescale of a satellite galaxy, provided  $M_{sat}$  is taken to be the total gaseous + dark matter mass of the satellite.

In our models, we use equation 10 to compute the timescale for an accreted satellite to reach the centre of the halo and merge with the central galaxy. The orbital eccentricity parameter  $\epsilon$  is drawn randomly from a uniform distribution from 0 to 1. The radius  $r_c$  is set equal to  $R_{vir}$ , the virial radius of the primary halo.  $M_{sat}$  is taken as the baryonic mass of the satellite plus the mass of its surrounding halo at the time it was last a central galaxy.

Note that it is assumed that satellite galaxies merge only with the central galaxy of the primary halo and only after time  $T_{dynf}$ . If the primary halo is later accreted by a larger system, new orbital parameters for all the remaining unmerged satellites are drawn, the dynamical friction timescales are recomputed and the merger clock is reset to zero. In practice, substructure in halos will not be erased immediately and for a while a satellite galaxy may still be able to merge with its old central object.

## 4.5 Formation of Elliptical Galaxies and Spiral Bulges

If two galaxies merge and the mass ratio between the satellite and the central object is greater than 0.3, we add the stars of both objects together and create a bulge component. If  $M_{sat}/M_{central} < 0.3$ , we add the stars and cold gas of the satellite to the disk component of the central galaxy. The value of 0.3 is motivated by a series N-body simulations of merging disk galaxies of unequal mass (Barnes, private communication). When a bulge is formed by a merger, all cold gas present in the two galaxies is transformed into stars in a “starburst” with a timescale of  $10^8$  years. Further cooling of gas in the halo may lead to the formation of a new disk.

The morphological classification of galaxies is made according their B-band disk-to-bulge ratios (Simien & de Vaucouleurs 1986). If  $M(B)_{bulge} - M(B)_{total} < 1$  mag, then the galaxy is classified as early-type (elliptical or S0).

It should be noted that although we track the formation of galaxies in halos as small as 10 particles, we do not accurately predict the morphologies of galaxies contained in such halos, simply because their merging histories are not resolved. Accurate morphologies are only obtained for central galaxies in halos with  $\sim 100$  particles, i.e. for galaxies with luminosities  $\sim L_*$ .

## 4.6 Stellar Population Models

We use the new stellar population synthesis models of Bruzual & Charlot (in preparation), which include updated stellar evolutionary tracks and new spectral libraries. In this paper, all stars are assumed to have solar metallicity. The star formation history of any galaxy can be approximated by a series of delta-function “bursts” of different masses. The stellar population models are used to generate lookup tables of the luminosity of a burst of fixed mass as a function of age in each photometric band. The magnitude of the galaxy at  $z = 0$  is calculated by summing the mass-weighted luminosities of each burst.

We have adopted a Scalo (1986) initial mass function with upper and lower mass cutoffs of  $100 M_\odot$  and  $0.1 M_\odot$ . As shown in Kauffmann & Charlot (1998), the stellar mass-to-light ratios of an old (8-10 Gyr) stellar population are then in good agreement with the observed mass-to-light ratios of elliptical galaxies within an effective radius.

## 4.7 Dust Extinction

In the models there is a strong distinction between central and satellite galaxies. Gas cools continuously onto central galaxies and they form stars at a roughly constant rate. Satellite galaxies lose their supply of new gas and, as a result, have exponentially declining star formation rates, leading to redder colours and lower gas fractions than central galaxies. A central galaxy is thus considerably brighter than a satellite companion of the same stellar mass at ultraviolet and optical wavelengths. As we will show in section 6.4, this influences the amplitude of the correlation function of galaxies selected according to B-band magnitude.

It is a well-known but oft-ignored observational fact that gas-rich, star-forming galaxies contain dust, which absorbs a substantial fraction of the light emitted in the short wavelength part of the spectrum and re-radiates it in the far-infrared. We include a simple, empirically-

motivated recipe for dust extinction in our models in order to investigate how much this effect can influence our estimates of clustering in the models.

Wang & Heckman (1996) have studied the correlation of the optical depth of dust in galactic disks with the total luminosity of the galaxy. They studied 150 normal late-type galaxies with measured far-ultraviolet (UV,  $\lambda \sim 2000\text{\AA}$ ) fluxes and compiled the corresponding far-infrared (FIR,  $\lambda \sim 40\text{--}120\mu\text{m}$ ) fluxes measured by the IRAS satellite. They then modelled the absorption and emission of radiation by dust with a simple model of a uniform plane-parallel slab in which the dust that radiates in the IRAS band is heated exclusively by UV light from nearby hot stars. They find that their observed UV-to-FIR ratios can be explained by the face-on extinction optical depth  $\tau$  varying with the intrinsic UV luminosity of the galaxy as

$$\tau \propto \tau_0 (L/L_*)^\beta, \quad (11)$$

with  $\beta \sim 0.5$ . The same scaling law was also able to account for the  $H\beta/H\alpha$  ratios measured for a subset of the galaxies. Re-expressed in the blue-band, Wang & Heckman derive a total extinction optical depth of  $\tau_{B,*} = 0.8 \pm 0.3$  at the fiducial observed blue luminosity of a Schechter  $L_*$  galaxy ( $M_*(B) = -19.6 + 5 \log h$ ).

We use the Galactic extinction curve of Cardelli, Clayton & Mathis (1989) to derive  $\tau_\lambda/\tau_B$ . Although the extinction curves of smaller, less-metal rich galaxies such as the LMC and SMC are quite different at ultraviolet wavelengths, at optical wavelengths they are all fairly similar. This leads to face-on extinction for an  $L_*$  disk galaxy of 0.9, 0.8, 0.4 and 0.08 mag in the B, V, I and K bands respectively.

Finally, one must also take into account the inclination of the galaxy to the line-of-sight when making an extinction correction. For a thin disk where dust and stars are uniformly mixed, the total extinction in magnitudes is

$$A_\lambda = -2.5 \log \left( \frac{1 - e^{-\tau_\lambda \sec \theta}}{\tau_\lambda \sec \theta} \right). \quad (12)$$

In our dust-corrected models, we apply an extinction correction to every galaxy forming stars at a rate greater than  $0.5 M_\odot \text{yr}^{-1}$ . We use  $M_*(B) = -19.6 + 5 \log h - 0.9$  in equation 11, and scale  $\tau_\lambda$  using the *uncorrected* B-magnitudes predicted by the model. We then pick a random inclination for each galaxy and apply the final correction using equation 12.

## 4.8 Detailed Implementation of the Prescriptions

In the simulation, each galaxy carries a number of “labels” corresponding to different physical properties. These are:

1.  $M_*$ , total stellar mass
2.  $M_*(\text{bulge})$ , stellar mass of the bulge component
3.  $M_{\text{cool}}$ , cold gas mass
4.  $L(B, V, R, I, K\dots)$ , total present-day luminosity in a given waveband
5.  $L_{\text{bulge}}(B, V, R, I, K\dots)$ , the present-day bulge luminosity

Satellite galaxies carry two additional labels:

1.  $t_{merg}$ , the time until the satellite galaxy should merge with the central object.
2.  $i_{merg}$ , the index of the halo in which the satellite resided at the previous timestep.

In the ejection feedback scheme, each *halo* carries an array  $M_{eject}(M_{prog})$ , which is the amount of gas ejected by galaxies in progenitor halos of mass  $M_{prog}$ .

At each output time, we loop over all the halos in the catalogue and follow a series of steps:

1. We re-incorporate gas that was ejected out of progenitor halos more than a factor of two less massive than the present halo
2. We calculate the mass of hot gas in the halo at the start of the timestep. This is given by

$$M_{hot} = \Omega_b M_{vir} - \sum_{gals} (M_{cool} + M_*) - \sum_{M_{prog}} M_{eject}(M_{prog}), \quad (13)$$

where  $\sum_{gals}$  is the sum over all galaxies in the halo. Note that this assumes that when halos merge with each other, all gas that is not already cooled is shock heated to the virial temperature of the new halo. The sum over  $M_{prog}$  extends only over those progenitors more massive than  $M_{vir}/2$ .

3. We loop through the satellite galaxies in the halo and update their merging timescales. If the satellite was not in the largest progenitor of the halo at the previous timestep, its merging clock is reset. If the galaxy is predicted to merge during the timestep, it is flagged. The time between the beginning of the timestep and the merging event is noted.
4. We then solve a set of coupled differential equations for the time evolution of the cold gas and stars in each of the galaxies in the halo. We adopt a small timestep for this calculation (there are typically 100 timesteps between each pair of simulation outputs). For central galaxies, the change of the cold gas component over time  $\Delta t$  is given by:

$$M_{cool}(t + \Delta t) = M_{cool}(t) - (\dot{M}_* + \dot{M}_{reheat} - \dot{M}_{cool})\Delta t, \quad (14)$$

where  $\dot{M}_{cool}$ ,  $\dot{M}_*$  and  $\dot{M}_{reheat}$  are given by equations 5,6 and 7(or 9) respectively. For satellite galaxies, the equation is the same except there is no source term from gas cooling in the halo. Infall of cold gas onto satellites is assumed to be *disrupted* as soon as they are accreted so that star formation within them continues only until their existing cold gas reservoirs are exhausted.

The stars formed during time  $\Delta t$  are added to  $M_*$ . We look up the present-day luminosity of a burst of mass  $\dot{M}_*\Delta t$  and age  $t$  in our population synthesis tables and update the luminosities of the galaxies. Finally, the hot gas mass of the halo at the end of the timestep is calculated using

$$M_{hot}(t + \Delta t) = M_{hot}(t) - \sum_{gals} (\dot{M}_{cool} - \dot{M}_{reheat})\Delta t. \quad (15)$$

Note that this is valid for retention feedback. For ejection feedback, reheated gas is added instead to  $M_{eject}(M_{vir})$ , where  $M_{vir}$  is the virial mass of the halo.

5. If a satellite is predicted to merge during the timestep  $\Delta t$ , its stars and gas are added to the central galaxy. If the mass of the satellite is greater than one-third the mass of the central object, we set the stellar mass of the bulge component equal to the mass of the central galaxy plus the mass of the merged satellite. All the cold gas in the merger remnant is converted into stars at a constant rate over  $10^8$  years. Stars that form in such a burst do not reheat or eject cold gas. In addition, we assume that the burst is decoupled from the evolution of rest of the galaxy, i.e. we set  $M_{cool} = 0$  in the above equations immediately after the merger takes place. Both assumptions are motivated by N-body simulations, which show that gas in merging disk galaxies quickly loses angular momentum and ends up in a dense knot at the very centre of the remnant, and that feedback has rather little effect (Barnes & Hernquist 1996).

## 4.9 Normalizing the Models

For a given set of cosmological initial conditions (including the baryon density  $\Omega_b$ ), there are two “free parameters” in our models – the star formation efficiency  $\alpha$  and the feedback efficiency  $\epsilon$ . As in KWG, we tune these two parameters to match the luminosity and cold gas mass of a fiducial reference galaxy, which we take to be the central galaxy in a halo with circular velocity  $V_c = 220 \text{ km s}^{-1}$ . In most previous work we have normalized the models using standard parameters for the Milky Way, but here, following the suggestions of Somerville & Primack (1998), we adopt a normalization that is consistent with the velocity-based zero-point of the I-band Tully-Fisher relation as determined by Giovanelli et al (1997). Matching to I-band rather than B-band data ought to be more robust, since the I-band is considerably less affected by dust extinction and star formation. Moreover, a very large amount of data on the I-band Tully-Fisher relation is now available. Giovanelli et al obtain the following fit, based on 555 galaxies in 24 clusters:

$$M_I - 5 \log h = -21.00 \pm 0.02 - 7.68 \pm 0.14(\log W - 2.5) \quad (16)$$

To convert between the measured  $HI$  line-widths  $W$  and the model circular velocities we assume  $W = 2V_c$ . In practice, there is substantial uncertainty in the relation between the circular velocity of the halo and that of the disk (e.g. Mo, Mao & White 1998), since the transformation between the two quantities depends on the detailed density profile of the halo and whether or not gas loses angular momentum before settling onto the disk. We set the parameters  $\alpha$  and  $\epsilon$  so that the central galaxy in a halo with  $V_c = 220 \text{ km s}^{-1}$  has  $M_I - 5 \log h \sim -22.1$  and a cold gas mass  $\sim 10^{10} M_\odot$ . It should be noted that this normalization is considerably brighter than that adopted by KWG, who took the observed B-band magnitude of the Milky Way to be  $B \sim -20.5$ . For a Hubble constant of  $50 \text{ km s}^{-1} \text{ Mpc}^{-1}$  and assuming  $B - I \sim 1.8$  for a spiral galaxy (De Jong 1996), the new normalization means that the central galaxy in a halo with  $V_c = 220 \text{ km s}^{-1}$  has a B-band magnitude of  $-21.8$  – more than a factor 3 more luminous than the observed value. Consistency of this Tully-Fisher normalization with the estimated magnitudes of our own Galaxy and of M31 is only obtained for substantially higher values of the Hubble constant, which do not give acceptable ages for a Universe with  $\Omega = 1$ .

The fact that there are only two free parameters in the model should not be interpreted as an indication that the physical processes governing galaxy formation are well-specified.

On the contrary, we will show that the way in which we choose to implement feedback and whether or not dust is included in the model can have a very large effect both on the luminosity function and on the amplitude of the correlation function on scales below a few Mpc. We will attempt to clarify how different parametrizations of these processes affect our results and which processes appear to be most critical if one is to succeed in matching the observational data.

## 5 Comparison of galaxy properties for semi-analytic and simulation merger trees

If halo merging trees derived using methods based on the extended Press-Schechter formalism (Cole 1991; Kauffmann & White 1993; Rodrigues & Thomas 1996 Somerville & Kolatt 1998) were statistically equivalent to the trees found in the N-body simulations, the same galaxy luminosity functions would be obtained using the two approaches, provided the same recipes for cooling, star formation and feedback were employed, and the same halo mass resolution limit was adopted. In practice, the halo mass function derived by the Press-Schechter argument does not fit very accurately the mass function in N-body simulations. For halo masses between  $10^{11}$  and  $10^{14} M_{\odot}$ , the Press-Schechter theory predicts roughly twice as many halos as are actually found in the GIF simulations for both the  $\tau$ CDM and the  $\Lambda$ CDM cosmologies. Most of the missing mass in the simulations is in the form of “unresolved” material – single particles or groups with less than 10 members. This discrepancy between the Press-Schechter and simulation mass functions propagates to the halo progenitor distributions and to the Monte-Carlo merging trees (Somerville, Lemson & Kolatt, in preparation).

Here we compare the the predictions of the two approaches for the luminosity functions of galaxies within halos of given mass and for the “field” luminosity function. In figure 2, we plot the number of galaxies brighter than a given V-magnitude in halos with circular velocity  $V_c$ . Solid squares show mean results derived using analytic trees constructed as described in Kauffmann & White (1993). Solid circles show results derived from the simulation. The error bars on the points show the rms scatter in the number of galaxies in halos of given circular velocity. We perform the comparison using the  $\tau$ CDM model and we use the *same* prescriptions (from KWG) for cooling, star formation, feedback, merging and stellar population synthesis in both cases. We truncate the analytic trees at a halo mass of  $2 \times 10^{11} M_{\odot}$  so that the resolution is the same as in the simulations. The four panels in figure 2 show the number of galaxies per halo brighter than  $M_V = -18, -19, -20$  and  $-21$ . As can be seen, the mean number of lower-luminosity galaxies per halo ( $M_V > -20$ ) agrees remarkably well. The analytic approach appears to overpredict the number of bright galaxies in high  $V_c$  halos by a factor of  $\sim 2$ , but since there are not many such halos in the simulation and the number of bright galaxies within them is small, the discrepancy may not be statistically significant.

Figure 3 compares the field luminosity functions derived using the semi-analytic trees and the simulations. The top panel shows the difference between the abundance of halos predicted by Press-Schechter theory, and that found in the simulation. The Press-Schechter overprediction of halo abundance at intermediate masses is quite evident. The middle panel compares the magnitude of the *central* galaxy as a function of halo circular velocity. There is good agreement between the two approaches. Note that the dip in magnitude at  $V_c = 500$

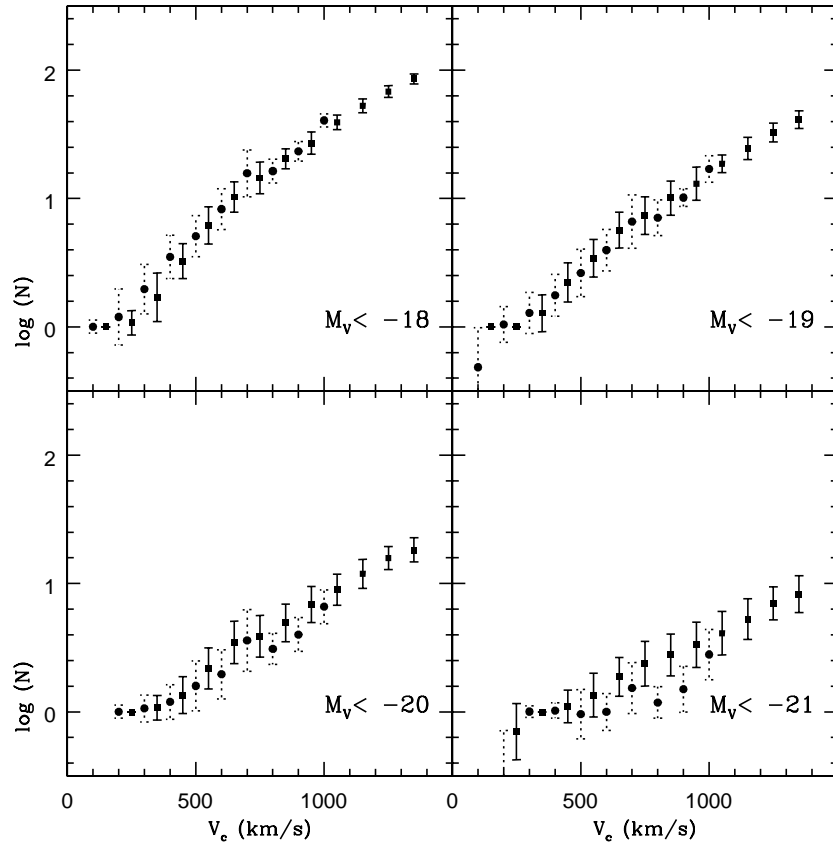


Figure 2: The number of galaxies brighter than a given V-magnitude in halos with circular velocity  $V_c$ . Solid circles show results derived using the analytic trees constructed as described in Kauffmann & White (1993). Solid squares show results derived from the simulation. Error bars show the rms deviation between the number of galaxies in different halos.

km s<sup>-1</sup> arises because we assume stars do not form in the cooling flows of halos with circular velocities greater than this value. The bottom panel compares the V-band “field” luminosity functions. Except perhaps near the “knee”, the agreement between the two approaches is excellent.

The comparison in this section demonstrates that although merging trees derived using the extended Press-Schechter theory differ in detail from those found in the simulations, the two methods give very similar results both for the mean number and luminosity of galaxies within halos, and for the scatter in these quantities.

## 6 Results of the Models

### 6.1 Slices from the simulation

In figure 4, we show slices of thickness  $8 h^{-1}$  Mpc from the  $\tau$ CDM simulation. The distribution of dark matter is shown in the top left panel. In the top right panel, all the galaxies in the slice with magnitudes brighter than  $M(B) = -19.0 + 5 \log h$  are plotted as solid white circles. Galaxies with magnitudes brighter than  $M(B) = -17.5 + 5 \log h$  are shown in the bottom panels. We divide these galaxies into two equal subsamples at the median star formation rate per unit stellar mass. The bottom left panel shows the distribution of galaxies with low star formation rates. The bottom right panel shows galaxies with high star formation rates.

Galaxies of all luminosities trace the filaments and knots visible in the dark matter distribution. Galaxies with high star formation rates are less clustered than galaxies with low star formation rates. Star-forming galaxies tend to avoid dense clusters and groups and occur more frequently in voids.

Figure 5 shows a similar set of slices from the  $\Lambda$ CDM simulation. The area and thickness of these slices have been chosen to have the same dimensions in *redshift space* as those in figure 4 ( $85h^{-1}$  Mpc  $\times$   $85h^{-1}$  Mpc  $\times$   $8h^{-1}$  Mpc). The same systematic effects are visible in the two figures and the most obvious difference between them is the difference in galaxy abundance. We return to this in section 6.3.

### 6.2 The Tully-Fisher Relation

As described in section 4.9, all models are normalized so that the average I-band magnitude of the central galaxy in a halo of circular velocity  $V_c = 220$  km s<sup>-1</sup> is  $-22.1 + 5 \log h$ , in accordance with the zero point of the I-band Tully-Fisher relation derived by Giovanelli et al. (1997). Figure 6 shows the Tully-Fisher relation for spiral galaxies in the simulations. We have selected central galaxies with  $1.5 < M(B)_{bulge} - M(B)_{tot} < 2.2$  (appropriate for Sb/Sc type galaxies). The solid line is the fit to the data (equation 16). The upper two panels show the  $\tau$ CDM model for the two different feedback prescriptions discussed in section 4.3. Although the slopes are similar, the ejection prescription results in considerably more scatter, particularly at low velocity widths, where there is a marked tail of low-luminosity galaxies. The lower panel shows the  $\Lambda$ CDM model with retention feedback. We do not show a  $\Lambda$ CDM model with ejection feedback as this model would result in too low a total luminosity density, as explained in the next section. It is interesting that the scatter obtained for both the  $\Lambda$ CDM and  $\tau$ CDM relations, even for retention feedback, is not much smaller than the

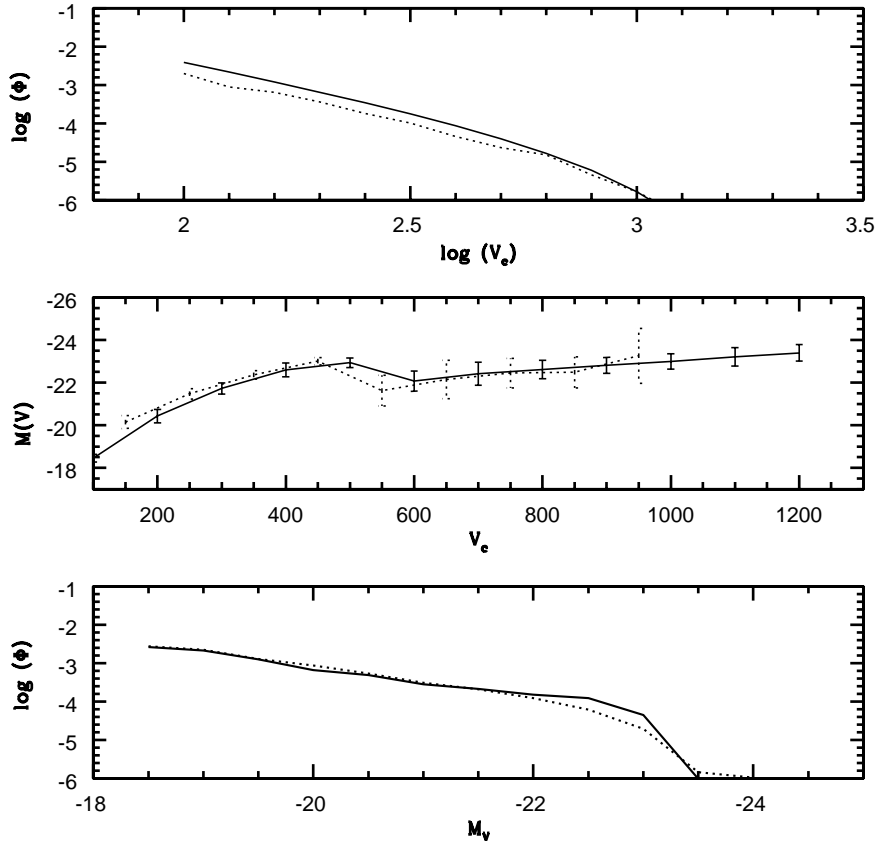


Figure 3: *Top panel:* A comparison of the abundance of halos as a function of circular velocity predicted by the Press-Schechter theory (solid) and the abundance derived from the simulation (dotted). *Middle panel:* Magnitude of the *central galaxy* as a function of halo circular velocity. Error bars show the rms scatter between halos. The Press-Schechter theory halos are solid and the simulation is dotted. *Bottom panel:* The V-band field luminosity functions derived using the Press-Schechter approach (solid) and the simulations (dotted).

Figure 4: Slices of thickness  $8 h^{-1}$  Mpc from the  $\tau$ CDM simulation. The distribution of dark matter is shown in the top left panel. In the top right panel, all galaxies with  $M(B) < -19.0 + 5 \log h$  are plotted as solid white circles. Galaxies with  $M(B) < -17.5 + 5 \log h$  are shown in the bottom panels. We divide these galaxies into two equal subsamples at the median star formation rate per unit stellar mass. The bottom left panel shows the distribution of galaxies with low star formation rates. The bottom right panel shows galaxies with high star formation rates.

Figure 5: Slices of thickness  $8 h^{-1}$  Mpc and length  $85 h^{-1}$  Mpc from the  $\Lambda$ CDM simulation. The panels are as described in figure 4.

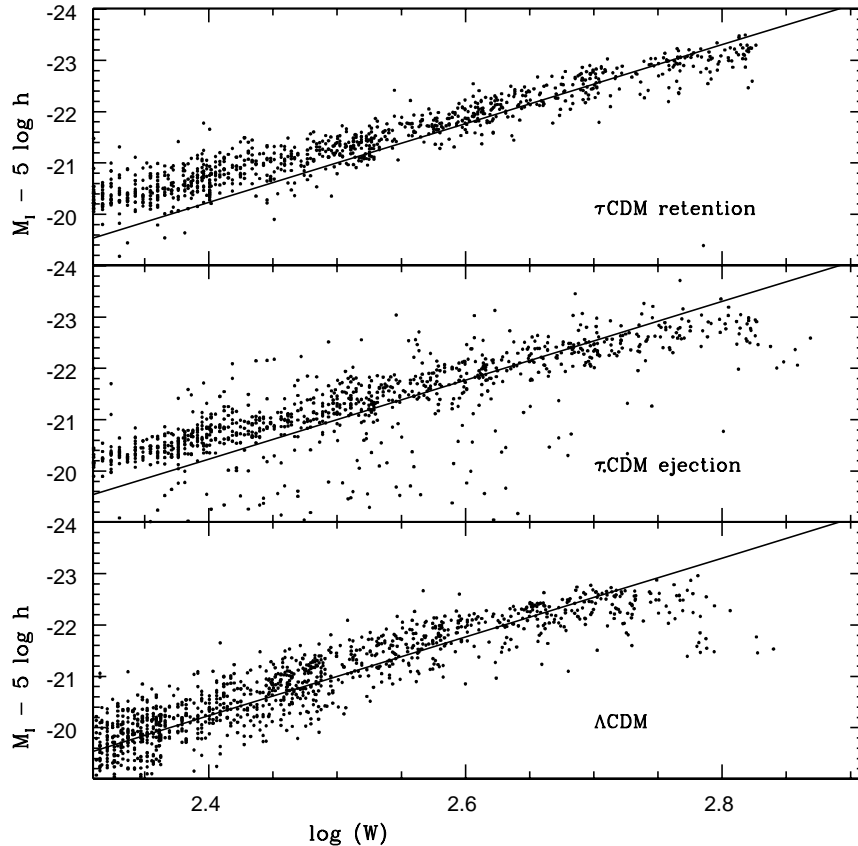


Figure 6: The I-band Tully-Fisher relation for spiral galaxies in the simulations. The solid lines show the relation of Giovanelli et al (1997).

observed scatter. The model scatter arises because of differences in star formation history and stellar mass between central galaxies in different halos of the same circular velocity. As pointed out by Mo, Mao & White (1998), scatter in the spin parameter of dark matter halos leads to a spread in contraction factors for disks forming in halos of a given circular velocity. Halos with high values of  $\lambda$  produce disks with rotation curves that are slowly rising, whereas halos with low values of  $\lambda$  produce disks with rotation curves that rise steeply and then decline. This leads to intrinsic scatter in the predicted Tully-Fisher relation even if disks in halos of given circular velocity are assumed to have fixed mass and mass-to-light ratio. This must be added to the scatter already visible in figure 6. More complex modelling is necessary to investigate these issues in detail.

### 6.3 The Luminosity Function

In figure 7, we show B-band luminosity functions for the  $\tau$ CDM simulation. A sequence of different models is shown in order to illustrate the effect of including different prescriptions for

feedback and dust extinction. The results are compared with the B-band luminosity functions derived from several recent redshift surveys: the APM-Stromlo survey (Loveday et al 1992), the Las Campanas Redshift Survey (LCRS) (Lin et al 1997) and the ESO-Slice survey (Zucca et al 1997). Note that we only plot the luminosity functions down to magnitudes where our simulations are “complete” (i.e. the luminosity of the central galaxy in a halo with 10 particles).

In the top left panel, we plot the luminosity function for a model with retention feedback and no dust extinction. In this case, the model luminosity function exceeds the observed one by more than a factor of 10 at all luminosities. The inclusion of dust brings the model more in line with the observations at luminosities around  $L_*$ , but there are still far too many galaxies at both fainter and brighter magnitudes. The model with ejection feedback agrees much better with the observations at  $L_*$  and below. This is because ejection feedback suppresses the formation of bright galaxies in low mass halos. The first generation of stars formed when the halo collapses generates enough energy to empty the halo of gas and halt further star formation. This process is only efficient in low-circular velocity systems, so the excess of galaxies brighter than  $L_*$  still remains a problem. Including dust in the ejection model (lower right panel) helps somewhat, but the predicted abundance of bright galaxies is still more than a factor 10 above the Schechter function representation of the observations.

In figure 8, we compare the model K-band luminosity functions with the Schechter fits derived by Gardner et al (1997) and Szokoly et al (1998) for two independent surveys. Unlike B-band magnitudes, the K-band luminosities of galaxies depend on their total stellar masses, rather than their present-day star formation rates. Moreover, K-magnitudes are only weakly affected by dust extinction. The fact that the model K-band luminosity functions also disagree with the data at the bright end shows that there are too many *massive* galaxies in the simulations.

B-band and K-band luminosity functions for the  $\Lambda$ CDM model are shown in figure 9. Retention feedback is assumed. Even so, this model produces a factor  $\sim 2 - 3$  too few galaxies at magnitudes around  $L_*$ . There is again an excess of very bright galaxies, but the problem is less severe than in  $\tau$ CDM. The same trends are apparent in the K-band.

In summary, the luminosity functions for both models have the wrong shape, with or without dust extinction. Instead of declining exponentially at bright magnitudes, they exhibit a gentler turn down. In previous work, KWG and Cole et al (1994) obtained much better fits to the bright end of the luminosity function (see also figure 3). As explained in section 4.9, this is because they adopted a much fainter normalization. If one is to obtain an exponential cutoff at high luminosities, bright galaxies must reside primarily in very massive halos on the exponentially declining part of the mass function. The shape problem is considerably worse for the  $\tau$ CDM model than for the  $\Lambda$ CDM model. Although both models are normalized to reproduce the observed abundance of rich clusters, the  $\tau$ CDM model has a higher abundance of intermediate mass halos than the  $\Lambda$ CDM model. It is the luminous galaxies in these halos that create the excess at magnitudes brighter than  $L_*$ . The  $\tau$ CDM model produces too many galaxies below  $L_*$  unless gas is efficiently ejected out of low mass halos. The  $\Lambda$ CDM model, on the other hand, produces too *few*  $L_*$  galaxies even if feedback is inefficient and if gas never escapes these halos.

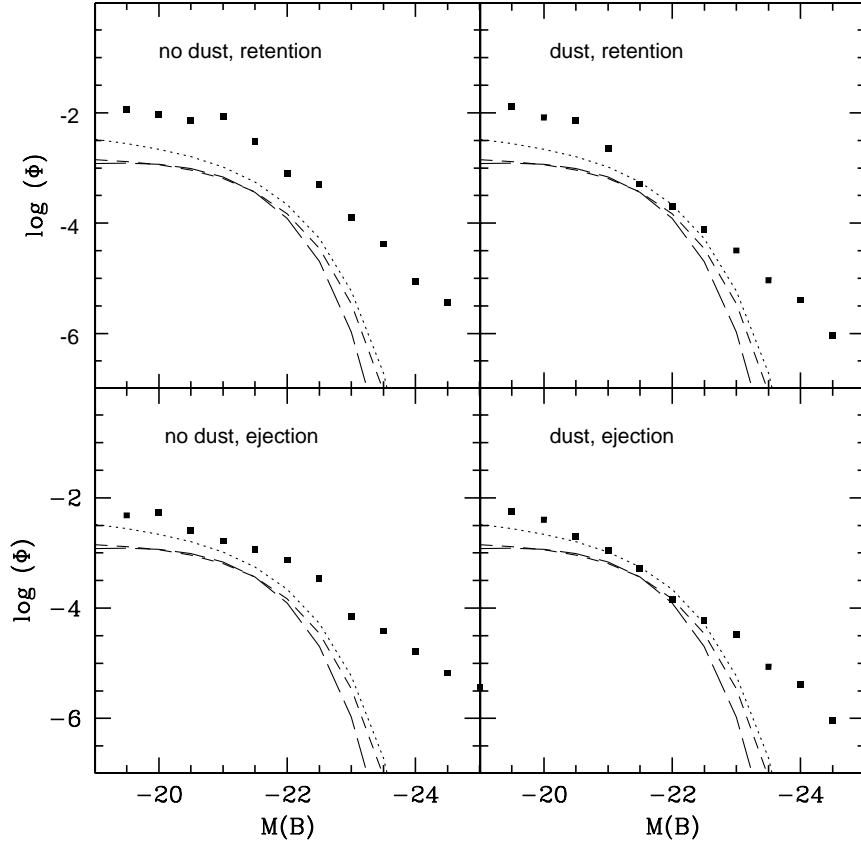


Figure 7: The B-band luminosity function for galaxies in the  $\tau$ CDM simulation. The four panels show models with different assumptions about feedback and dust extinction. The simulation results are shown as solid squares. The lines are Schechter fits to B-band luminosity functions from recent redshift surveys: 1) ESO-Slice (dotted), 2) APM-Stromlo (short-dashed), 3) LCRS (long-dashed).

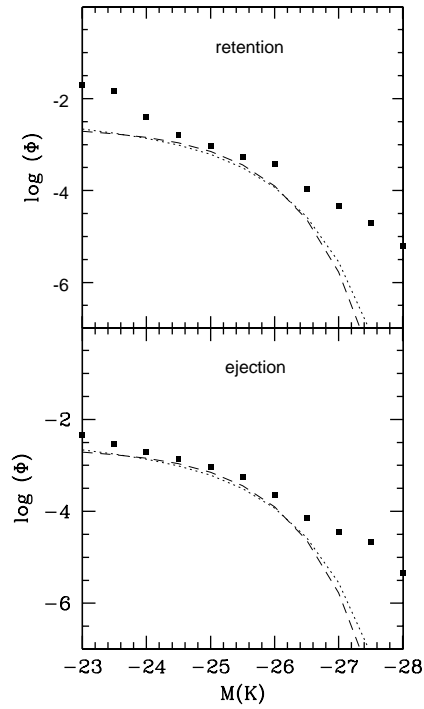


Figure 8: The K-band luminosity function for galaxies in the  $\tau$ CDM simulation. The two panels show models with different assumptions about feedback. Dust extinction is negligible in the K-band. The simulation results are shown as solid squares. The lines are Schechter fits to K-band luminosity functions derived by Gardner et al (dotted) and Szokoly et al (dashed)

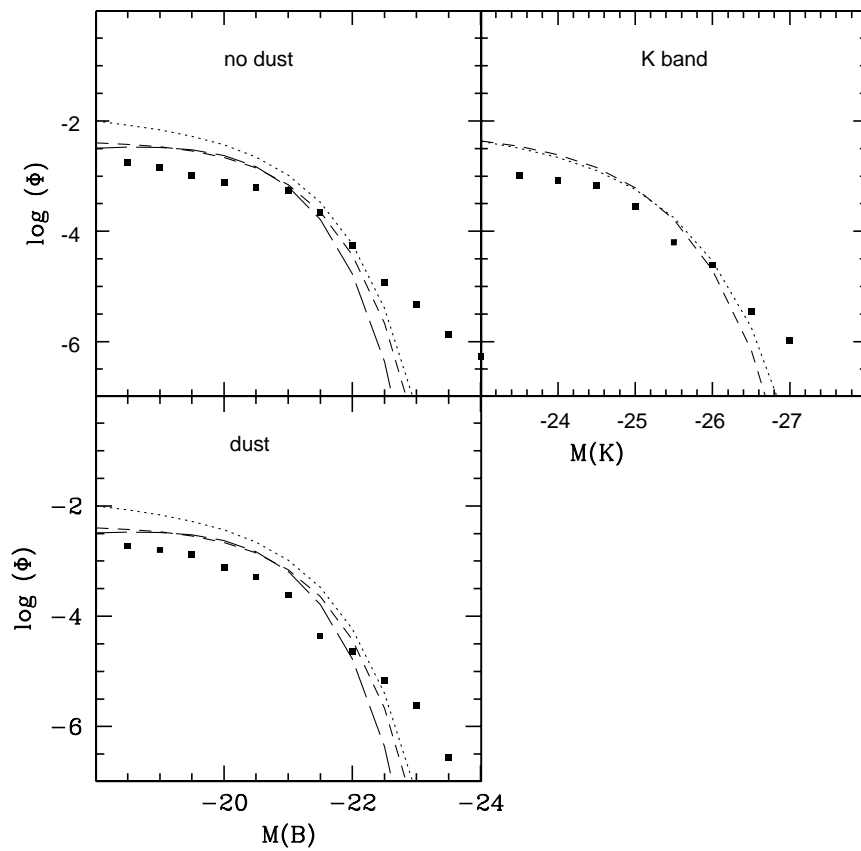


Figure 9: The B and K-band luminosity functions for galaxies in the  $\Lambda$ CDM simulation. The lines are as described in the previous two figures.

## 6.4 The Two-point Correlation Function

In figure 10, we show the galaxy two-point correlation function  $\xi(r)$  for the  $\tau$ CDM simulation. We select galaxies with B-band luminosities  $M(B) < -20.5$ . A sequence of models is again shown to illustrate different prescriptions for feedback and dust extinction. The results are compared with the real space correlation function measured from the APM galaxy survey (Baugh 1996).

For the model with retention feedback,  $\xi(r)$  follows a power law of slope  $\gamma \sim -1.7$  down to scales  $\sim 1$  Mpc, below which it flattens and then turns over. This is in marked contrast to the observed  $\xi(r)$ , which follows the same power law down to scales below 100 kpc. The inclusion of dust extinction lowers the luminosity of bright star-forming field galaxies and raises the amplitude of the correlation function on small scales, but  $\xi(r)$  still flattens and is a factor 6 below the observed value at  $r \sim 100$  kpc. As described in the previous section, ejection feedback suppresses bright star-forming galaxies in low circular velocity halos and brings the faint end of the luminosity function into better agreement with the observations. As seen in the bottom left panel of figure 10, ejection feedback also prevents  $\xi(r)$  from flattening below 1 Mpc. The results shown in the bottom right panel of figure 10, for the model with ejection feedback and dust extinction, agree rather well with the observations.

Figure 11 shows the galaxy two-point correlation function for the  $\Lambda$ CDM simulation. Retention feedback is assumed.  $\xi(r)$  does not turn over on small scales and the model with dust is actually *too steep* compared to observations.

What determines the slope and amplitude of the galaxy correlation functions in our models? In a recent paper, Mo & White (1996) developed a simple analytic model for the gravitational clustering of dark matter halos. The positions and formation times of halos were determined from the statistics of the initial linear density field and modifications caused by gravitationally-induced motions were treated using a spherical collapse approximation. Mo & White showed that on large scales, the halo autocorrelation function is simply proportional to the dark matter correlation function, with the constant of proportionality dependent on the masses of the selected halos. Because halos are spatially exclusive and have a finite radius, the halo-halo correlation function drops below the mass correlation function on scales comparable to the diameter of typical halos in the sample. From these results, it follows that if there is only one bright galaxy per halo, the galaxy correlation function will simply follow the form of the halo correlation function, with a flattening and turnover on scales less than  $\sim 1$  Mpc. In order for the galaxy correlation to continue as a power law to small scales, a substantial fraction of bright galaxies must exist as groups *within the same halo*.

This is illustrated quantitatively in figure 12, where we plot the fraction of galaxies in the simulation with  $M(B) < -20.5$  that occur in halos of a given circular velocity. The  $\tau$ CDM model with retention feedback has a much higher fraction of galaxies in low  $V_c$  halos than the  $\tau$ CDM model with ejection feedback. Low  $V_c$  halos typically contain only one bright galaxy (see figure 2), whereas high  $V_c$  halos contain many bright galaxies that contribute to clustering amplitude on sub-megaparsec scales. Figure 12 shows that there is a relatively small fraction of bright galaxies in low  $V_c$  halos in the  $\Lambda$ CDM model, even with retention feedback. Recall that both  $\tau$ CDM and  $\Lambda$ CDM are normalized to fit the observed number density of rich clusters at the present day. Because the mass density in the  $\Lambda$ CDM model is lower, the number density of low mass halos is also smaller.  $\Lambda$ CDM thus “naturally” has more galaxies

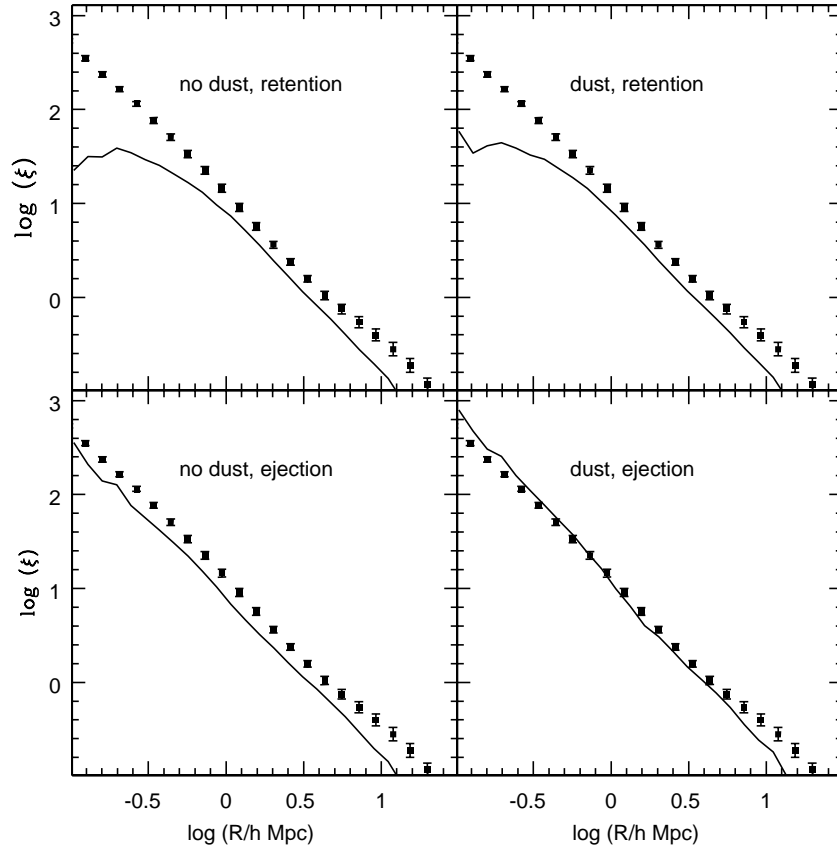


Figure 10: The two-point correlation function  $\xi(r)$  for galaxies in the  $\tau$ CDM simulation. Solid lines show the simulation results for different prescriptions for feedback and dust extinction. The points with error bars are taken from Baugh (1995).

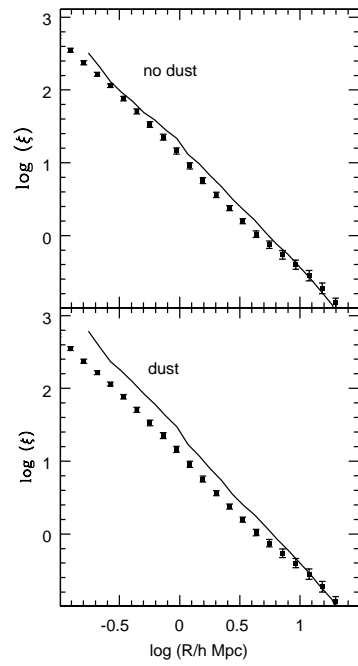


Figure 11: The two-point correlation function  $\xi(r)$  for galaxies in the  $\Lambda$ CDM simulation (solid line). Points are observational data from the APM survey.

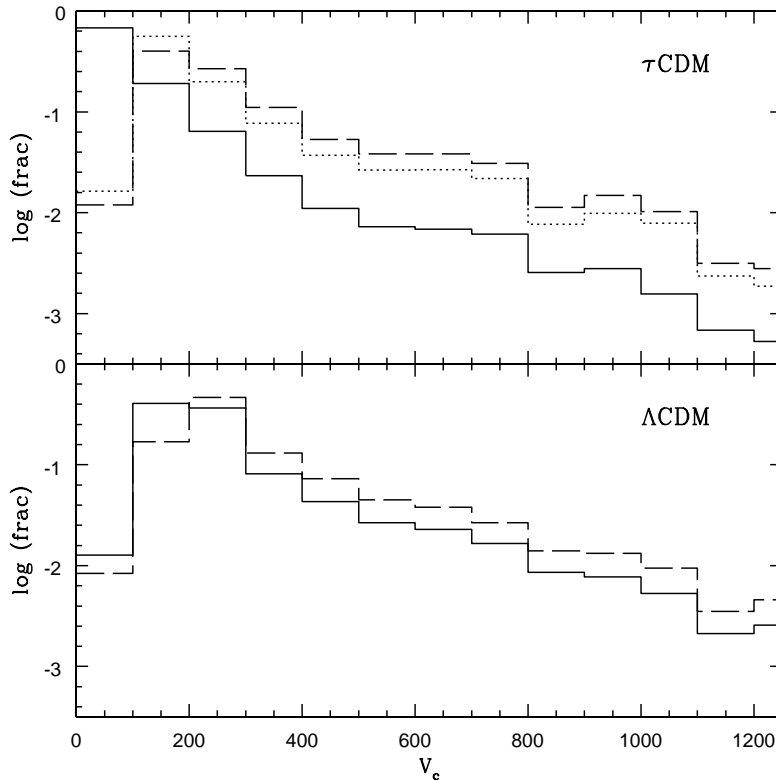


Figure 12: The fraction of galaxies in the simulation with  $M(B) < -20.5$  that occur in halos of a given circular velocity. *Upper panel:*  $\tau$ CDM, retention feedback (solid), ejection feedback (dotted), ejection feedback + dust (dashed). *Lower panel:*  $\Lambda$ CDM, retention feedback (solid), retention feedback + dust (dashed).

in clusters relative to the field and as a result,  $\xi(r)$  is steep on small scales.

## 6.5 Pairwise Velocity Moments

Figure 13 shows the first ( $v_{12}$ ) and the second moment ( $\sigma_{12}$ ) of the one-dimensional radial pairwise velocity distribution of galaxies and dark matter particles as a function of pair separation for our best-fit models. Bold lines are the moments for the dark matter particles. Solid and dotted lines are the moments for galaxies brighter than  $M_B = -17.5 + 5 \log h$  and  $M_B = -18.5 + 5 \log h$ , respectively. Brighter cutoffs yield similar results. Galaxies do not show any significant velocity bias on any non-linear scale regardless of their luminosity. This result is not trivial because galaxies are not a random subsample of dark matter particles. This result is consistent with the weak density bias and the lack of luminosity segregation described in Sect. 6.6.

The pairwise velocity dispersion profile  $\sigma_{12}(r)$  is sensitive to the presence of clusters within the sample and therefore to the total volume of the sample. Our simulation box has a volume

of the order of  $10^6 h^{-3} \text{ Mpc}^3$  which is comparable to the volume  $\sim 7 \times 10^5 h^{-3} \text{ Mpc}^3$  within  $cz = 12000 \text{ km s}^{-1}$  of the northern slice of the Center for Astrophysics Redshift Surveys (hereafter CfA2N, de Lapparent et al 1991; Geller & Huchra 1989; Huchra et al 1990; Huchra et al 1995). Filled squares in figure 13 show  $\sigma_{12}(r)$  for the CfA2N slice. Both  $\tau$ CDM and  $\Lambda$ CDM models are in remarkably good agreement with the CfA2N slice.

Lacking the full three-dimensional information, we compute the CfA2N values by fitting the redshift space correlation function  $\xi(r_p, \pi)$  with the convolution model (Fisher 1995): we model  $\xi(r_p, \pi)$  as the convolution of the real space correlation function with an exponential pairwise velocity distribution (Davis & Peebles 1983; details of this procedure are given in Marzke et al 1995). In order to apply this procedure, we need to assume a model for the mean streaming velocity  $v_{12}(r)$ . We adopt the similarity solution suggested by Davis & Peebles (1983)  $v_{12}(r) = r/[1+(r/r_0)^2]$  where  $r_0 = 5.83h^{-1} \text{ Mpc}$  is the CfA2N galaxy-galaxy correlation length. Assuming  $v_{12}(r) = 0$  usually yields lower values of  $\sigma_{12}$  (see e.g. Marzke et al 1995; Somerville, Primack & Nolthenius 1997). Note that our simulations show  $v_{12} \sim 200 - 300 \text{ km s}^{-1}$  at relative separations  $r \sim 1h^{-1} \text{ Mpc}$  and do not support the assumption of a null  $v_{12}(r)$ .

In future papers, we use mock redshift surveys to show that this procedure yields pairwise velocity dispersion profiles  $\sigma_{12}(r)$  in reasonably good agreement with the real profile. It is therefore encouraging that the  $\sigma_{12}(r)$  profiles of our best-fit models match the CfA2N result.

## 6.6 Galaxy Bias

An important issue we wish to address is that of galaxy “bias”, i.e. whether the clustering amplitude of the galaxies in our models differs from that of the underlying dark matter. In figure 14, we compare  $\xi(r)$  for galaxies of different luminosities, morphological types and colours with  $\xi(r)$  for the dark matter. For  $\tau$ CDM, we show the model with ejection feedback and dust extinction and for  $\Lambda$ CDM, we show the model with retention feedback and dust extinction. These are the “best fit” models in both cases.

On large scales, galaxies of all luminosities are unbiased in both models. On small scales, the  $\tau$ CDM galaxies are slightly more clustered than the dark matter, whereas the  $\Lambda$ CDM galaxies are a factor  $\sim 2 - 3$  less clustered. Neither model displays any luminosity segregation; galaxies of all magnitudes cluster in the same way. As discussed by Kauffmann, Nusser & Steinmetz (1997), positive bias is obtained for galaxies in halos more massive than  $M_*(z = 0)$ , the mass of the typical collapsed object at the present day. For cluster-normalized CDM models,  $M_*$  is large ( $\sim 10^{14} M_\odot$ ). Our bright normalization also causes luminous galaxies to be placed in relatively low mass halos. This is why we do not see the luminosity-dependent bias discussed by Kauffmann, Nusser & Steinmetz (1997).

On the other hand, red galaxies and to a lesser extent early-type galaxies are more clustered than the underlying population, particularly on small scales. These galaxies occur preferentially in the cores of groups and clusters (see figures 4 and 5). Conversely, star-forming galaxies are less clustered on small scales because they are predominantly central halo galaxies and are thus spatially exclusive. A similar result can be seen in the earlier work of Cen & Ostriker (1992).

The relative bias between different types of galaxies in the Southern Sky Redshift Survey has recently been analyzed in a paper by Willmer, Da Costa & Pellegrini (1998). These authors find that galaxies with magnitudes below  $\sim L_*$  do not exhibit any luminosity-dependent

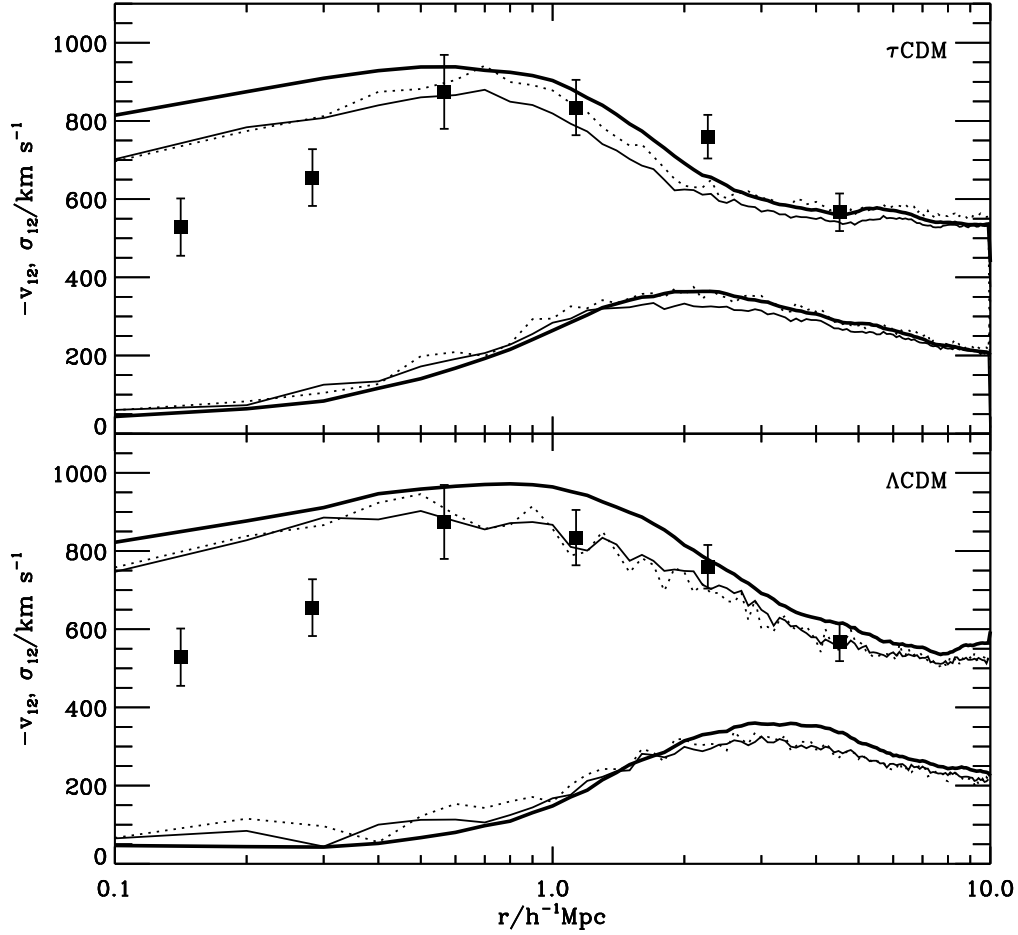


Figure 13: Mean streaming velocity  $v_{12}$  (lower curves) and pairwise velocity dispersion  $\sigma_{12}$  (upper curves) at different relative separations for our best-fit models. Bold, solid, and dotted lines are the moments for the dark matter particles, galaxies brighter than  $M_B = -17.5 + 5 \log h$  and  $M_B = -18.5 + 5 \log h$ , respectively. Solid squares are the pairwise velocity dispersions for the CfA2N redshift survey. Error bars are computed with a bootstrap resampling method.

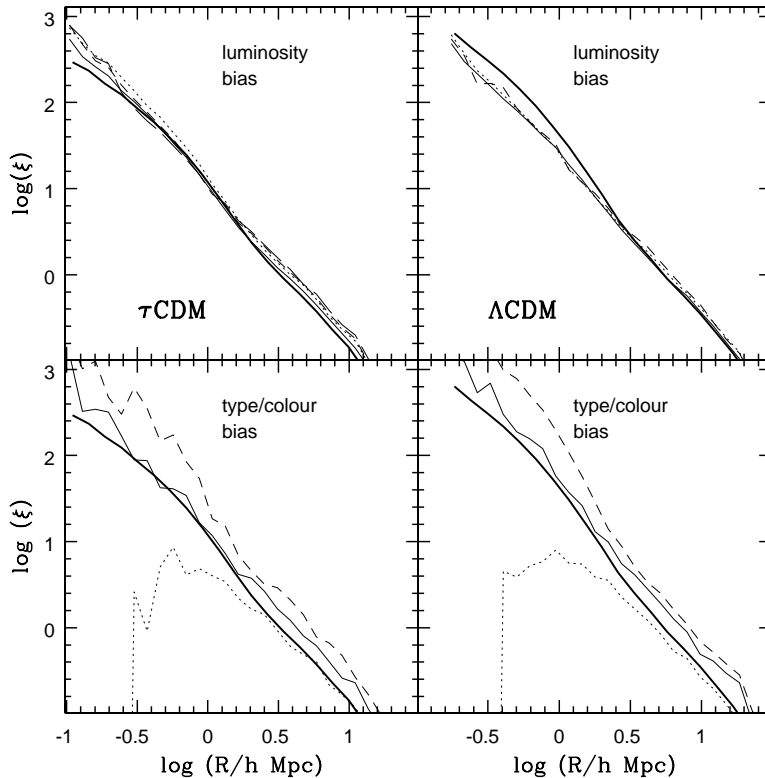


Figure 14: Galaxy bias as a function of luminosity, type, colour and star formation rate. The left panels are for the  $\tau$ CDM simulation, the right panels are for the  $\Lambda$ CDM simulation. *Upper panels:* The thick solid line is the dark matter correlation function. Thin solid lines show  $\xi(r)$  for different B-band luminosities:  $B < -19$  (solid),  $B < -20$  (dotted),  $B < -20.5$  (short-dashed),  $B < -21$  (long-dashed). *Lower panels:* Thick solid line is the dark matter correlation function. Thin solid line corresponds to early-type galaxies, dashed line to red ( $B - V > 0.8$ ) galaxies, and dotted line to star forming ( $SFR > 2M_{\odot} \text{ yr}^{-1}$ ) galaxies.

bias, but at magnitudes brighter than  $L_*$ , galaxies are significantly more strongly clustered ( $b(L > L_*)/b(L_*) = 1.5$ ). As discussed above, our models do not exhibit this luminosity-dependent bias, perhaps indicating that our adopted normalization is too bright. Willmer, Da Costa & Pellegrini also find that both early-type galaxies and red galaxies cluster more strongly than the galaxy population as a whole. The bias is stronger on small scales ( $r < 4 h^{-1}$  Mpc) than on larger scales. In addition, galaxies with *colours* characteristic of old stellar populations exhibit more bias than galaxies with early-type morphologies. These results are in good qualitative agreement with the results shown in figure 14 and the earlier results of Kauffmann, Nusser & Steinmetz (1997).

## 6.7 Mass-to-light Ratios of Clusters

Clusters of galaxies are the largest collapsed objects in the universe and have often been used as a means of estimating the cosmological density parameter  $\Omega$ . The standard procedure is as follows. The mass of a cluster within some radius is measured using techniques such as galaxy kinematics, X-ray profiles or gravitational lensing. This is compared to the luminosity within the same radius to calculate a mass-to-light ratio. The mean mass density of the universe is then estimated by multiplying its mean luminosity density by this number. The validity of this technique depends on two questionable assumptions:

1. Luminosity is “conserved” when field galaxies fall into a cluster. In practice, we know that cluster galaxies are predominantly ellipticals with no ongoing star formation, whereas field galaxies are predominantly spirals in which stars are forming at several solar masses per year. The stellar mass-to-light ratios of field and cluster galaxies thus differ strongly at optical and UV wavelengths.
2. The efficiency of galaxy formation is the same in all environments.

Most studies of cluster mass-to-light ratios give values corresponding to  $\Omega \sim 0.2$  (see for example Carlberg et al 1996). If a high-density cosmology is to be consistent with these observations, we require the mass-to-light ratios of clusters to be significantly *lower* than the mass-to-light ratio of the Universe as a whole. This is often also referred to as “bias” in the literature, though this kind of bias is quite different to what we measure when we compare the correlation functions of galaxies and dark matter.

Figure 15 shows the mass-to-light ratios of our simulated halos divided by the mass-to-light ratio of the simulation as a whole. The results are shown as a function of the virial mass of the halo and for both B and I-bands. It is interesting that in the  $\Omega = 1$   $\tau$ CDM model, the mass-to-light ratios of clusters *are* significantly lower than the global value. The factor ( $\sim 2$ ) that we obtain is somewhat too small, however, to bring the model into good agreement with the observations. Rich clusters in the  $\Lambda$ CDM model have mass-to-light ratios only 10-20 % smaller than the global value. It is also interesting that groups of galaxies are predicted to have lower mass-to-light ratios than clusters in both models. This agrees with the observed trends.

## 6.8 Colour Distributions

We now compare the  $B - V$  colour distributions of our model galaxies with colours of bright nearby galaxies in the RC3 catalogue (De Vaucouleurs et al 1991). We have selected 1580 galaxies with  $M_B < -19.0 - 5 \log h$ , which have both morphological classifications and magnitudes in the Johnson  $B$  and  $V$ -bands. Of these galaxies, 653 are classified as early-type. Note that the fraction of early-type galaxies is rather high, which may reflect the fact that the sample is dominated by galaxies in the Virgo cluster. In our simulation  $\sim 25\%$  of galaxies to this magnitude limit have  $M(B)_{bulge} - M(B)_{total} < 1$  mag and so are classified as early types.

In figure 16, we compare the colour distributions of galaxies in the  $\tau$ CDM model with that of the RC3 sample. The left panel shows the model with ejection feedback, but without any dust extinction. The right panel shows the same model with dust extinction. Without dust extinction, the model colour distribution peaks at  $B - V \sim 0.6$  in contrast to the observed

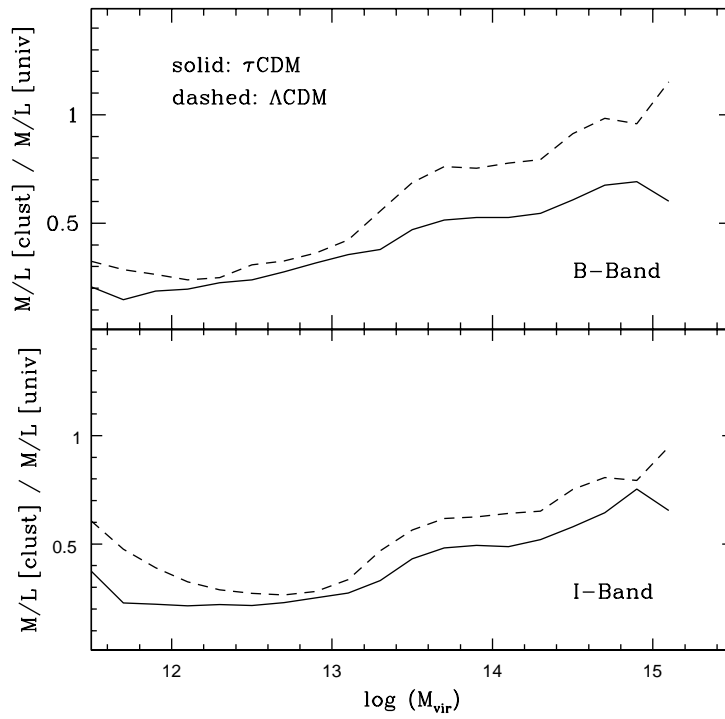


Figure 15: The mass-to-light ratios of halos divided by the mass-to-light ratio of the Universe as a whole. The results are shown as a function of the virial mass of the halo.

distribution, which is relatively flat from  $B - V \sim 0.4$  to  $B - V \sim 1$ . In particular, early-type galaxies appear to be significantly too blue in this model. With the inclusion of dust, the color distribution broadens significantly. Many of the field ellipticals on our models have a lower-luminosity, star-forming disk component. The inclusion of dust in the models reddens these objects and brings the colour distribution of early-type galaxies into better agreement with the observations.

The colour distributions of galaxies in the  $\Lambda$ CDM models are shown in figure 17. Because galaxies form earlier in this cosmology, the colours tend to be redder on average, but the effect is small. Again, the effect of dust extinction is to broaden the colour distributions and to bring them into better agreement with the observations.

## 6.9 Star Formation Rate Functions

In addition to the luminosity function and the colour distributions of galaxies, observational estimates of the number density of galaxies as a function of star formation rate provide an important constraint on galaxy formation theories. Gallego et al (1995) have analyzed a complete sample of emission-line galaxies and have computed an  $H\alpha$  luminosity function. Assuming a Scalo (1986) IMF and using Case B recombination theory to predict the luminosity of the  $H\alpha$  emission line for a given rate of star formation, they derive an integrated star formation rate density of the local Universe of  $0.013 \pm 0.001 M_{\odot} \text{yr}^{-1} \text{Mpc}^{-3}$  (for  $H_0 = 50 \text{ km s}^{-1} \text{Mpc}^{-1}$ ).

In figure 18, we compare the  $H\alpha$  luminosity functions of our models with the results of Gallego et al. We have used the same transformation as these authors to convert from star formation rate to  $H\alpha$  luminosity,

$$L(H\alpha) = 9.40 \times 10^{40} \frac{SFR}{M_{\odot} \text{yr}^{-1}} \text{ergs s}^{-1}. \quad (17)$$

The results of the  $\tau$ CDM model agree better with the observations than those of the  $\Lambda$ CDM model. For  $\tau$ CDM, we obtain an integrated SFR density of  $0.017 M_{\odot} \text{yr}^{-1} \text{Mpc}^{-3}$ . For  $\Lambda$ CDM the present-day SFR density is a factor  $\sim 4$  too low. From figure 18, we see that there is a lack of galaxies forming stars at rates between 1 and  $10 M_{\odot} \text{yr}^{-1}$ . These are the same galaxies that are missing at the “knee” of the B-band luminosity function in figure 9.

## 7 Discussion and Conclusions

None of the models analyzed in this paper provides a completely satisfactory fit to all the observed properties of galaxies at  $z = 0$ . If supernova feedback is weak, the  $\Omega = 1$   $\tau$ CDM model produces too high a total luminosity density. Most of the excess luminosity is in the form of star-forming “field” galaxies. As a result, the galaxy correlation function turns over on scales below a few Mpc. The observed two-point correlation function, on the other hand, is well represented by a single power law of slope  $-1.7$  down to scales approaching 10 kpc (Baugh 1996). If one assumes instead that supernova feedback is able to eject gas out of a halo, so that it becomes unavailable for further cooling and star formation until much later times, the number of star-forming galaxies in low-mass field halos is significantly lowered and

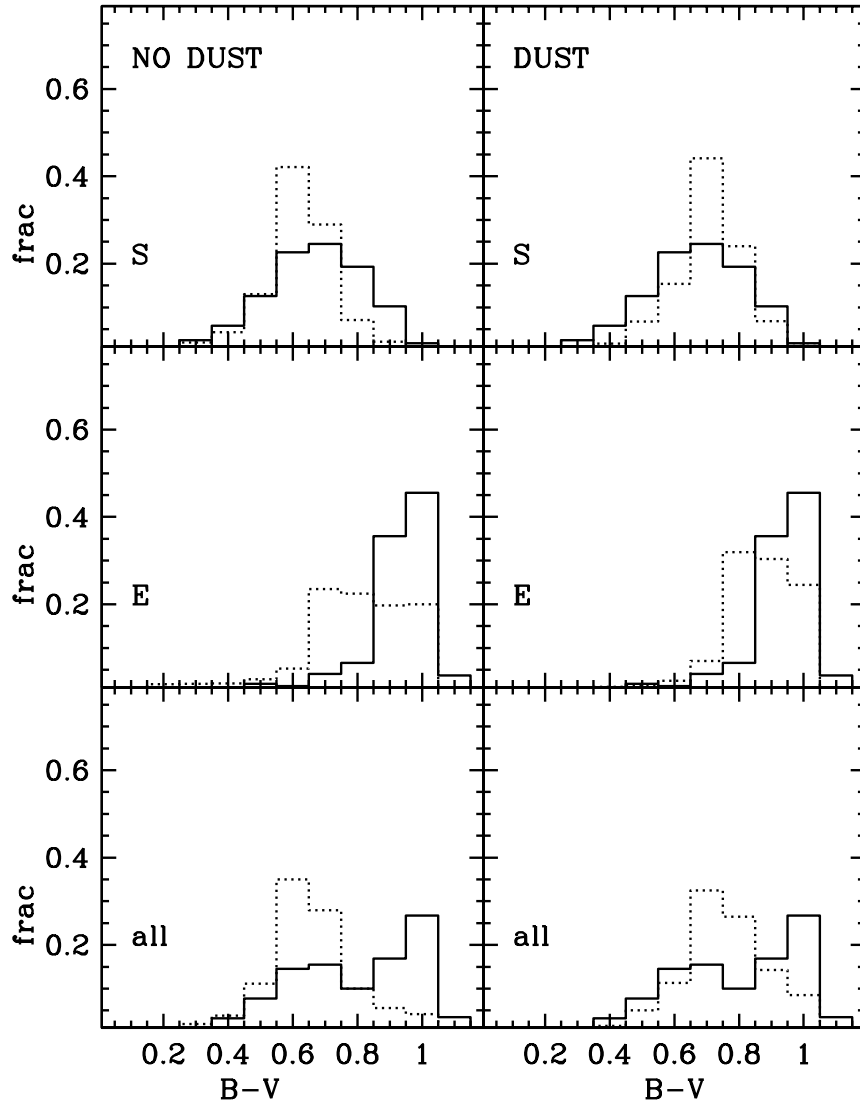


Figure 16: The  $B - V$  colour distribution of galaxies brighter than  $B = -20.5$  in the  $\tau$ CDM simulation. The left panel shows a model without dust and the right panel a model with dust. Dotted lines show the model distributions. Solid lines show the distribution of  $B < -20.5$  galaxies with both colours and morphologies in the RC3 catalogue.

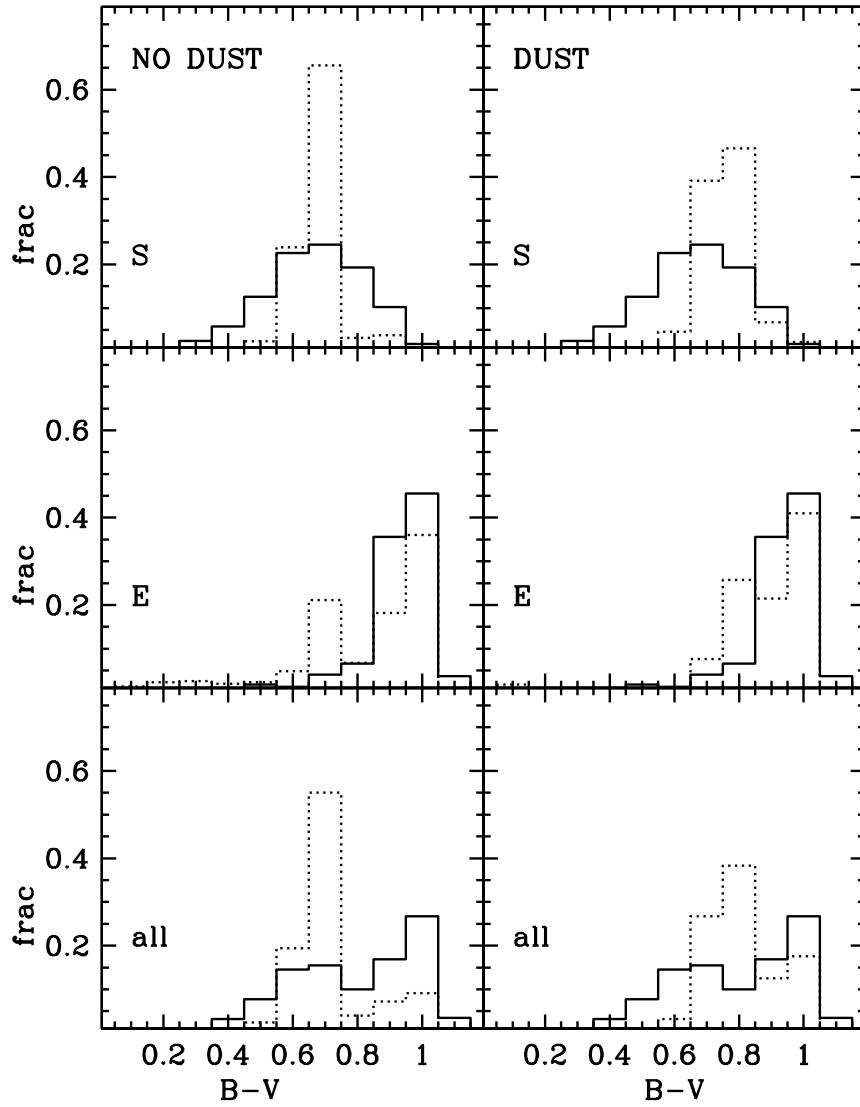


Figure 17: The  $B - V$  colour distribution of galaxies brighter than  $B = -19.7$  in the  $\Lambda$ CDM simulation. The left panel shows a model without dust and the right panel a model with dust.

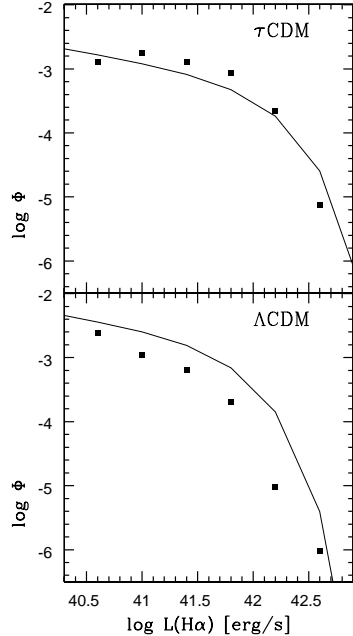


Figure 18: The H $\alpha$  luminosity function of galaxies in the simulation compared to the Schechter fit derived by Gallego et al (1995).

this improves the fit to the observed luminosity and correlation functions. Even so, the model still produces an excess of very bright galaxies in groups and clusters. The  $\Omega = 0.3$   $\Lambda$ CDM model has the opposite problem: it produces too few  $L_*$  galaxies, even if feedback is weak and no gas leaves the halo. The two point correlation function is also too steep on scales below a few Mpc.

One obvious inference we can draw from these results is that a CDM model with density parameter somewhere between 0.3 and 1 may well do better in matching the observations. Indeed, in recent work, Somerville & Primack (1998) find that a model with  $\Omega = 0.5$  provides the best fit.

Care must be exercised, however, before drawing strong conclusions about cosmological parameters. Many of our difficulties in fitting the observed shape of the galaxy luminosity function come about because we have chosen a very bright normalization for the models. This is because we *force* the models to fit the zero-point of the Giovanelli et al I-band Tully-Fisher relation at a circular velocity of  $V_c = 220 \text{ km s}^{-1}$ . We have also assumed that the circular velocities of central disk galaxies are the same as those of their surrounding halos. In practice, the relation between the circular velocities of disk and halo is not straightforward and requires a detailed model for the internal structure of the halo and of the galaxy within it. More detailed calculations of disk formation in CDM halos predict that the circular velocity of the disk is generally *higher* than that of the surrounding halo (Mo, Mao & White 1998). This results in a higher total luminosity density for the same Tully-Fisher normalization, and would improve the fit of the  $\Lambda$ CDM model while making the  $\tau$ CDM model even more discrepant.

One might also question whether normalizing the models to match the Tully-Fisher relation is sensible, since the physical origin of this relation is still uncertain and depends on structural properties of the galaxies which we are not attempting to model. We have argued that the distribution of K-band luminosities should provide a robust test of galaxy formation theory, since the K-band luminosity of a galaxy depends primarily on its stellar mass and not on its instantaneous star formation rate or its dust content. With the advent of wide-field K-band galaxy surveys such as the Two Micron All Sky Survey (2MASS, Kleinmann et al 1994), normalizing the models to match the observed K-band luminosity function may be the best choice for the future.

Another effect we have investigated is that of dust extinction in star-forming galaxies. If dust is ignored, the  $\Omega = 1$   $\tau$ CDM model produces too many blue galaxies compared to the observations. Galaxy formation occurs rather late in this model, so the stellar populations of galaxies are younger than in the  $\Lambda$ CDM model. However, the inclusion of a simple, empirically-motivated dust extinction scheme makes this problem go away, and the colour distributions of galaxies in the  $\tau$ CDM and  $\Lambda$ CDM models are then virtually indistinguishable. Since dust extinction only affects star-forming field galaxies, models with dust produce somewhat steeper and higher amplitude correlation functions. Finally, dust lowers the predicted number of galaxies at the bright end of the B-band luminosity function. Our models tend to produce a power-law “tail” of high-luminosity galaxies, rather than a sharp exponential cutoff. Although dust can reduce this tail in the B-band, the problem persists in the K-band.

Finally, although we have tried to illustrate the effect of different schemes for star formation, feedback and dust, we cannot be sure that we have taken into account all the key physical processes that may seriously affect our results. For example, we have proposed that very efficient feedback can stop galaxies forming in low-mass halos, but alternative schemes may be possible. For example, Jimenez et al (1997) have proposed that the gaseous disks that form in low  $V_c$  halos are not subject to the instabilities that cause star formation and are thus not seen in the optical or UV, although their emission at 21 cm wavelengths should be detectable. The only way to make progress is through observational studies of how star formation rates, cold gas and dust contents, and the shells and bubbles seen around star-forming regions, vary with galactic mass, metallicity, morphology and environment. This is a massive and long-term undertaking, but it seems necessary if we are to build a picture of galaxy formation that is more than just schematic.

We conclude that we cannot reliably constrain the values of cosmological parameters using the properties of the galaxy distribution at  $z = 0$  because our results are strongly influenced by our adopted normalization and the way in which we choose to parametrize star formation and supernova feedback. The main effects of changing the cosmological parameters in our set of cluster-normalized CDM models are

1. to shift the epoch when halos of a given mass form
2. to change the number density of galactic-mass halos at the present day.

The adopted normalization and the recipes for feedback and star formation affect the efficiency with which stars form as a function of redshift and galaxy mass. It is thus not surprising that there is considerable freedom to “tune” our results to fit the observations. Nevertheless it is interesting that very different star formation and feedback schemes are required to come

close to reproducing the observations in the two cosmologies we have explored. For  $\Omega = 1$ , we require that feedback be very efficient at removing gas both from galaxies and from their surrounding halos. Many lower-mass halos are “dark” in this model, containing a faint, possibly low-surface brightness object. In a low-density Universe, feedback must be inefficient and every halo must contain a star-forming galaxy if we are to match the observations. This gives us confidence that if the cosmological parameters of the Universe can be determined using techniques such as the analysis of small-scale fluctuations in the microwave background (e.g. Bond, Efstathiou & Tegmark 1997) or the light-curves of high-redshift supernovae (e.g. Perlmutter et al 1997), the methodology introduced in this paper will become valuable for understanding and constraining the detailed physical processes operating within galaxies.

It is also encouraging that our best-fit models come reasonably close to fitting many different observed measures of the galaxy distribution *at the same time*. The models that give the best fits to the B-band luminosity function, also give the best fits to the K-band luminosity function, the correlation function, the color distribution and the star formation rate function. In Paper II we demonstrate that these same models provide a reasonably good match to the observed properties of galaxy groups. This gives us confidence that the fundamental theoretical framework, which determines how galaxy properties scale with halo mass, may indeed be correct.

## Acknowledgments

The simulations in this paper were carried out at the Computer Center of the Max-Planck Society in Garching and at the EPPC in Edinburgh. Codes were kindly made available by the Virgo Consortium. We especially thank Adrian Jenkins and Frazer Pearce for help in carrying them out. We are also grateful to Margaret Geller, John Huchra and Ron Marzke for enabling us to compare the CfA2N data directly with the simulations. A.D. is a Marie Curie Fellow and holds grant ERBFMBICT-960695 of the Training and Mobility of Researchers program financed by the EC.

Table 1: Cosmological parameters of the GIF models.  $\Omega_0$  and  $\Omega_\Lambda$  are the density parameters for matter and for the cosmological constant,  $h$  is the Hubble parameter,  $\sigma_8$  is the rms of the density field fluctuations in spheres of radius  $8 h^{-1}$  Mpc, and  $\Gamma$  is the shape parameter of the power spectrum. Also given is the size of the cosmological simulation box.

Model	$\Omega_0$	$\Omega_\Lambda$	$h$	$\sigma_8$	$\Gamma$	Box Size [Mpc/ $h$ ]
SCDM	1.0	0.0	0.5	0.60	0.50	85
$\tau$ CDM	1.0	0.0	0.5	0.60	0.21	85
$\Lambda$ CDM	0.3	0.7	0.7	0.90	0.21	141
OCDM	0.3	0.0	0.7	0.85	0.21	141

## References

- Allen, S.W. & Fabian, A.C., 1997, MNRAS, 286, 583
- Barnes, J.E. & Hernquist, L., 1996, ApJ, 471, 155
- Bartelmann, M., Huss, A., Colberg, J.M., Jenkins, A. & Pierce, F.R., 1998, A&A, 330, 1
- Baugh, C.M., Cole, S. & Frenk, C.S., 1996a, MNRAS, 282, 27
- Baugh, C.M., Cole, S. & Frenk, C.S., 1996b, MNRAS, 283, 1361
- Baugh, C.M., 1996, MNRAS, 280, 267
- Baugh, C.M., Cole, S., Frenk, C.S. & Lacey, C., 1998, ApJ, 498, 504
- Binney, J. & Tremaine, S., 1987, Galactic Dynamics, Princeton University Press
- Bond, J.R., Efstathiou, G. & Tegmark, M., 1997, MNRAS, 291, 33
- Bond, J.R., Cole, S., Efstathiou, G. & Kaiser, N. 1991, ApJ, 379, 440
- Bower, R.J., 1991, MNRAS, 248, 332
- Bower, R.G., Coles, P., Frenk, C.S. & White, S.D.M., 1993. ApJ, 405, 403
- Cardelli, J.A., Clayton, G.C. & Mathis, J.S., 1989, ApJ, 345, 245
- Carlberg, R.G. Couchman, H.M.P. & Thomas, P., 1990, ApJ, 352, L29
- Carlberg, R.G., Yee, H.K.C., Ellingson, E., Abraham, R., Gravel, P., Morris, S. & Pritchet, C.J., 1996, ApJ, 462, 32
- Cen, R. & Ostriker, J.P., 1992, ApJ, 393, 22
- Cen, R. & Ostriker, J.P., 1993, ApJ, 417, 415
- Cole, S., 1991, ApJ, 367, 45
- Cole, S., Aragón-Salamanca, A., Frenk, C.S., Navarro, J.F. & Zepf, S.E., 1994, MNRAS, 271, 781

Couchman, H.M.P., Thomas, P.A. & Pearce, F.R., 1995, ApJ, 452, 797

Davis, M. & Peebles, P.J.E., 1983, ApJ, 267, 465

De Jong, S., 1996, A&AS, 118, 557

De Lapparent, V., Geller, M.J. & Huchra, J.P., 1991, ApJ, 369, 273

De Vaucouleurs, G., De Vaucouleurs, A., Corwin, H.G., Buta, R.J., Paturel, G. & Fouque, P., 1991, Third Reference Catalogue of Bright Galaxies, Springer-Verlag

Eke, V.R., Cole, S. & Frenk, C.S., 1996, MNRAS, 282, 263

Evrard, A.E., Summers, F.J. & Davis, M., 1994, ApJ, 422, 11

Fabian, A.C., Nulsen, P.E.J. & Canizares, C.R., 1991, A&ARv, 2, 191

Ferland, G.J., Fabian, A.C. & Johnstone, R.M., 1994, MNRAS, 266, 399

Fisher, K.B., 1995, ApJ, 448, 494

Frenk, C.S., Evrard, E.E., White, S.D.M. & Summers, F.J., 1996, ApJ, 472, 460

Gallego, J., Zamorano, J., Aragon-Salamanca, A. & Rego, M., 1995, ApJ, 455, L1

Gardner, J.P., Sharples, R.M., Frenk, C.S. & Carrasco, B.E., 1997, ApJ, 480, 99

Geller, M.J. & Huchra, J.P., 1989, Science 246, 897

Ghigna, S., Moore, B., Governato, F., Lake, G., Quinn, T. & Stadel, J., 1998, MNRAS, in press

Giovanelli, R.M., Haynes, M.P., Da Costa, L.N., Freudling, W., Salzer, J.J. & Wegner, G., 1997, ApJ, 477, L1

Governato, F., Baugh, C.M., Frenk, C.S., Cole, S., Lacey, C.G., Quinn, T. & Stadel, J., 1998, Nature, 392, 359

Heyl, J.S., Cole, S., Frenk, C.S. & Navarro, J.F., 1995, MNRAS, 274, 755

Huchra, J.P., de Lapparent, V., Geller, M.J. & Corwin, H.G., 1990, ApJS, 72, 433

Huchra, J.P., Geller, M.J. & Corwin, H.G., 1995, ApJS, 70, 687

Jimenez, R., Heavens, A.F., Hawkins, M.R.S. & Padoan, P., 1997, MNRAS, 292, L5

Katz, N., Hernquist, L. & Weinberg, D.H., 1992, ApJ, 399, L109

Kauffmann, G. & White, S.D.M., 1993, MNRAS, 261, 921

Kauffmann, G., White, S.D.M. & Guiderdoni, B. 1993, MNRAS, 264, 201 (KWG)

Kauffmann, G., Guiderdoni, B. & White, S.D.M., 1994, MNRAS, 267, 981

Kauffmann, G., 1995a, MNRAS, 274, 153

Kauffmann, G., 1995b, MNRAS, 274, 161

Kauffmann, G., 1996a, MNRAS, 281, 487

Kauffmann, G., 1996b, MNRAS, 281, 475

Kauffmann, G., Nusser, A. & Steinmetz, M., 1997, MNRAS, 286, 795

Kauffmann, G. & Charlot, S., 1998, MNRAS, 294, 705

Kennicutt, R.C., 1998, ApJ, 498, 541

Kleinman, S.G., Lysaght, M.G., Pughe, W.L., Schneider, S., Skrutskie, M.F., Weinberg, M.D., Price, S.D., Matthews, K., Soifer, B.T. & Huchra, J.P., 1994, Ap&SS, 217, 11

Klypin, A.A., Gottloeber, S., Kravtsov, A.V. & Khokhlov, A.M., 1998, ApJ, submitted

Lacey, C. & Silk, J., 1991, ApJ, 381, 14

Lacey, C. & Cole, S., 1993, MNRAS, 262, 627

Lacey, C., Guiderdoni, B., Rocca-Volmerange, B. & Silk, J., 1993, ApJ, 402, 15

Lin, H., Kirshner, R.P., Schechtman, S.A., Landy, S.D., Oemler, A., Tucker, D.L. & Schechter, P.L., 1997, ApJ, 464, 60

Loveday, J., Peterson, B.A., Efstathiou, G. & Maddox, S.J., 1992, ApJ, 390, 338

Marzke, R.O., Geller, M.J., Da Costa, L.N. & Huchra, J.P., 1995, AJ, 110, 477

Mo, H.J. & White, S.D.M., 1996, MNRAS, 282, 347

Mo, H.J., Mao, S. & White, S.D.M., 1998, MNRAS, 295, 319

Navarro, J.F. & White, S.D.M., 1994, MNRAS, 267, 401

Navarro, J.F., Frenk, C.S. & White, S.D.M., 1995, MNRAS, 275, 56

Navarro, J.F., Frenk, C.S. & White, S.D.M., 1996, ApJ, 462, 563

Peacock, J.A. & Dodds, S.J., 1994, MNRAS, 267, 1020

Pearce, F.R. & Couchman, H.M.P., 1997, New Astronomy, 2, 411

Perlmutter, S., Gabi, S., Goldhaber, G., Goobar, A., Groom, D.E., Hook, I.M., Kim, A.G., Kim, M.Y. et al., 1997, ApJ, 484, 565

Rodrigues, D.D.C. & Thomas, P.A., 1996, MNRAS, 282, 631

Roukema, B.F., Peterson, B.A., Quinn, P.J. & Rocca-Volmerange, B., 1997, MNRAS, 292, 835

Scalo, J.M., 1986, Fundamentals of Cosmic Physics, 11, 3

Simien, F. & De Vaucouleurs, G., 1986, ApJ, 302, 564

Somerville, R.S., Davis, M. & Primack, J.R., 1997, ApJ, 479, 616

Somerville, R.S., Primack, J.R. & Nolthenius, R., 1997, ApJ, 479, 606

Somerville, R.S. & Kolatt, T., 1998, MNRAS, in press

Somerville, R.S. & Primack, J.R., 1998, MNRAS, submitted

Szokoly, G.P., Subbarao, M.U., Connolly, A.J. & Mobasher, B., 1998, ApJ, 492, 452

Tormen, G., 1998, MNRAS, submitted

Tormen, G., Diaferio, A. & Syer, D., 1998, MNRAS, in press

Van Kampen, E. & Katgert, P., 1997, MNRAS, 289, 327

Viana, P.T.P. & Liddle, A.R., 1996, MNRAS, 281, 323

Wang, B. & Heckman, T.M., 1996, ApJ, 457, 645

White, S.D.M., Davis, M., Efstathiou, G. & Frenk, C.S., 1987, Nature, 330, 451

White, S.D.M. & Frenk, C.S., 1991, ApJ, 379, 52

White, S.D.M., Efstathiou, G. & Frenk, C.S., 1993, MNRAS, 262, 1023

White, M., Gelmini, G. & Silk, J., 1995, Phys.Rev.D, 51, 2669

Willmer, C.N.A., Da Costa. N. & Pellegrini, P.S., 1998, AJ, 115, 869

Zucca, E., Zamorani, G., Vettolani, G., Cappi, AS., Merighi, R., Mignoli, M., Stirpe, G.M.,  
Macgillivray, H. et al., 1997, A&A, 326, 477

This figure "fig04.gif" is available in "gif" format from:

<http://arxiv.org/ps/astro-ph/9805283v1>

This figure "fig05.gif" is available in "gif" format from:

<http://arxiv.org/ps/astro-ph/9805283v1>